

AMERICAN UNIVERSITY OF BEIRUT

ASSESSMENT OF AIRWAYS GEOMETRIC
MODELS BASED ON GAS TRANSPORT TO
THE BLOOD

by
ALI ZEIN SAAB

A thesis
submitted in partial fulfillment of the requirements
for the degree of Master of Engineering
to the Department of Mechanical Engineering
of the Faculty of Engineering and Architecture
at the American University of Beirut

Beirut, Lebanon
August 2019

AMERICAN UNIVERSITY OF BEIRUT

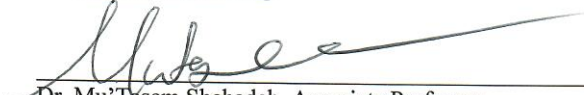
ASSESSMENT OF AIRWAYS GEOMETRIC
MODELS BASED ON GAS TRANSPORT TO
THE BLOOD

by
ALI ZEIN SAAB

Approved by:



Dr. Issam Lakkis, Professor
Mechanical Engineering
Advisor



Dr. Mu' Tasem Shehadeh, Associate Professor
Mechanical Engineering
Member of Committee



Dr. Salah Zeineldine, Professor (Associate)
Internal Medicine
Member of Committee



Dr. Daniel Tartakovsky, Professor
Energy Resources-Stanford University
Member of Committee

Date of thesis/dissertation defense: August 15, 2019

AMERICAN UNIVERSITY OF BEIRUT

THESIS, DISSERTATION, PROJECT
RELEASE FORM

Student Name: Saab Ali Zein
Last First Middle

Master's Thesis Master's Project Doctoral Dissertation

I authorize the American University of Beirut to: (a) reproduce hard or electronic copies of my thesis, dissertation, or project; (b) include such copies in the archives and digital repositories of the University; and (c) make freely available such copies to third parties for research or educational purposes.

I authorize the American University of Beirut, to: (a) reproduce hard or electronic copies of it; (b) include such copies in the archives and digital repositories of the University; and (c) make freely available such copies to third parties for research or educational purposes after: **One** **year from the date of submission of my thesis, dissertation or project.**
Two ___ years from the date of submission of my thesis, dissertation or project.
Three ___ years from the date of submission of my thesis, dissertation or project.

 9/6/2019
Signature Date

This form is signed when submitting the thesis, dissertation, or project to the University Libraries

Acknowledgements

I would like to thank Professor Lakkis for being there step by step through the whole Masters program;As he has been the main factor behind me being here today. Also, I would also like to show my genuine gratitude for everyone who supported me and stick out with me through it all. A special thanks for my dad, for he is the only person that I owe everything Iam today. Not to forget the members of the committee as they were very responsive and supportive.

An Abstract of the Thesis of

Ali Zein Saab for Master of Engineering
Major: Mechanical Engineering

Title: Assessment Of Airways Geometric Models Based On Gas Transport To The Blood

Engineers need to understand the respiratory process in order to design machines and medicines to help doctors deal with patients whose respiratory system function incorrectly or with difficulty. For this purpose we worked on developing the AUB pulmonary model by updating and validating this model and creating an automated interface tool that facilitates our model's usage. The main aim of our work was using this model to carry out assessment of existing airways network models. Topological structure of bronchial trees controls transport of gases and aerosols in the respiratory system. We start by providing a quantitative assessment of the alternative tree representations' ability to predict observable geometric and mechanistic characteristics, such as network resistance, dead space volume, and path length. Then we present a model of dynamic transport of oxygen and carbon dioxide along the airways, in the alveoli, across the alveolar membrane, and along the pulmonary blood capillaries. The model also accounts for the exchange of these two gases with blood in the capillaries, as well as age, gender and other in-species characteristics. Our model's predictions are compared with corresponding observations, providing an addition venue to assess the validity of the existing representations of the lung's bronchial tree.

Contents

Acknowledgements	v
Abstract	vi
1 Introduction	2
2 Review of the tracheobronchial tree	5
3 Our model	11
3.1 The mechanical model	11
3.2 The species transport model	14
3.2.1 Gas transport in the airways	15
3.2.2 Gas transport in the alveoli	15
3.2.3 Gas transport in the pulmonary membrane	17
3.2.4 Gas transport in the blood	18
3.3 Numerical Implementation of the Model	20
4 Results	22
4.1 Discussion	29
A Model Parameters	31
A.1 Nominal mass and height	32
A.2 Respiration Frequency	34
A.3 Trachea and main bronchi: length and diameter	35
A.4 The Number of Alveoli	37
A.5 Lung Volumes	40
A.5.1 Tidal volume	40
A.5.2 Functional Residual Capacity	41
A.5.3 Dead Space	44
A.6 Lung Mechanical Model Parameters	46
A.6.1 Compliance	46
A.6.2 Resistance	47

List of Figures

2.1	Airways generation length, normalized by the length of the trachea, vs the generation order for adults.	8
2.2	Airways generation diameter, normalized by the diameter of the trachea, vs the generation order for adults.	9
2.3	Airways generation length, normalized by the length of the trachea, vs the generation order for infants.	9
2.4	Airways generation diameter, normalized by the diameter of the trachea, vs the generation order for infants.	10
3.1	(a) circuit representation of a general airways mechanical model. (b) a simplified model.	12
3.2	Time variation of the pressure signal and the total alveolar volume under normal breathing conditions for an adult.	14
3.3	$\Delta p - V$ curve of the lung hysteresis.	14
3.4	Species transport in the airways.	15
3.5	Each terminal branch is connected to a number of alveoli. Our model assumes that the bronchiole is connected to the center of each compliant spherical alveolus.	16
4.1	Comparison of the time variation of the mean partial pressure of Oxygen (left) and carbon dioxide (right) in the blood and in the alveolar space of adults for selected airways geometry models.	25
4.2	Comparison of the time variation of the mean partial pressure of Oxygen (left) and carbon dioxide (right) in the blood capillary of adults for the different airways geometry models.	26
4.3	Comparison of the time variation of the mean partial pressure of Oxygen (left) and carbon dioxide (right) in the blood capillary of infants for the different airways geometry models.	26
4.4	Variation of the oxygen and carbon dioxide partial pressured in the blood along the capillary over one complete cycle (period T) for adults using the airways geometry in [1].	29
4.5	Variation of the oxygen and carbon dioxide partial pressured in the blood along the capillary over one complete cycle (period T) for infants using the airways geometry in [2].	29

A.1	Nominal mass versus age.	32
A.2	Nominal height versus age.	33
A.3	Nominal infant mass versus age.	33
A.4	Nominal infant height versus age.	34
A.5	Frequency of respiration versus age.	35
A.6	Trachea diameter versus age. [3] reported length and diameter of trachea vs age for 130 children and adolescents. [4]: 808 patients (430 males and 378 females).	36
A.7	Trachea length versus age. [5]: $\text{length(cm)}=0.0856*\text{height(cm)}-2.32$. [3] reported length and diameter of trachea vs age for 130 children and adolescents.	36
A.8	Number of alveoli vs age from various references.	38
A.9	Number of alveoli vs age from various references.	39
A.10	Number of alveoli per unit lung volume vs total lung volume from various references.	39
A.11	Nominal tidal volume versus age.	41
A.12	Functional residual capacity versus body height (measurements and relations). Converting from total lung volume to FRC is done by using the correlation by [6] of FRC dependence on lung volume and age, as plotted in Figure A.13.	43
A.13	Lung volume fractions as a function of age [6].	43
A.14	Dead space volume versus body length from [7],[8],[9]. When needed, growth charts were used to express height as a function of age.	45

List of Tables

2.1	Length (L) and diameter (D), both in mm, of the n th bronchi generation, predicted with tree models A–G for human adults. Model A [2] infers $L \sim n^{-1.38}$ and $D \sim n^{-1.26}$ from data; Model B [10] $L \sim \exp(-0.92n)$ and $D \sim \exp(-0.39n)$ for $n \leq 3$, and $L \sim \exp(-0.17n)$ and $D \sim \exp(-0.29n + 0.01n^2)$ for $n > 3$; Model D [11] $D \sim a^{25-n}$ with $a > 1$ varying between three groups of bronchi characterized by three intervals of n ; and Model E [12] identifying a linear relation, for each generation, between bronchi's length & diameter and human height H , $L \sim H$ and $D \sim H$. The remaining tree models, C [13], F [1] and G [14], fit no curves to the data reported therein.	6
2.2	Length (L) and diameter (D), both in mm, of the n th bronchi generation, predicted with the tree models A [2], E [12], and H [15] for human infants.	7
4.1	Baseline cases and model parameters values.	22
4.2	Comparison of the airways geometries in terms of dead space (DS), resistance (\mathcal{R}), total path length (L), time needed to reach saturation of oxygen in blood (T_r), mean oxygen partial pressure in blood ($\overline{P_{O_2}}$), and mean carbon dioxide partial pressure in blood ($\overline{P_{CO_2}}$). M: independently measured values. † corresponds to spatial averages along the capillary by assuming that P_{O_2} increases from 40 to 100 and P_{CO_2} decreases from 46 to 40 over one third of the capillary length. Partial pressures are in units of cmH_2O	23

4.3	Comparison of the airways geometries in terms time constant (τ), number of airways generations (N_g), length and diameter of the last generation channels (L_{N_g} and D_{N_g}), the ratio of the airways inlets diameter per alveolus to the alveolar diameter, (R_{in}/R_{alv}), Reynolds number in the last generation ($\text{Re}_{N_g} = \frac{\rho \bar{u}_{N_g} D_{N_g}}{\mu}$), and Peclet number in the last generation ($\text{Pe}_{N_g} = \frac{L_{N_g} \bar{u}_{N_g}}{\mathcal{D}}$). ρ is the density, μ is the viscosity, \mathcal{D} is the diffusion coefficient of species in air, f . The mean speed is estimated based by assuming that the lung changes its volume by the tidal volume (TV) over half a breath period ($1/(2f)$), i.e. $\bar{u}_{N_g} = (2TV f)/2^{N_g-1}$	24
A.1	Model parameters.	31
A.2	Data collected on number of alveoli in healthy subjects from different sources. gwk stands for gestation weeks. pnwk: postnatal weeks.	38
A.3	Data collected on FRC for both genders from different sources. M: male, F: female, P: plethysmography, MS: Mass spectrometry, U: Ultra sonic, H: Helium dilution, W: Washout.	42
A.4	Correlations for DS , DSE and DSP . Note that the $DSI = DS - DSE$. DSP : Physiological dead space. A: Asthmatic, CF: Cystic fibrosis, I: Intubated with cuffed endotracheal tubes, V: Ventilated.	44
A.5	Measurements of the dead space volume for adults (m : men, w : women).	45
A.6	Measurements of the dead space volume for infants. *calculated from age dependent correlations. P: Preterm birth. V: Ventilated.	46
A.7	Measurements of total resistance, dead space volume, and inductance for adults (m : men, w : women).	47
A.8	Measurements of total resistance, dead space volume, and inductance for infants. **Inspiration-Expiration. P: Preterm birth.	48

Nomenclature

Δp	Pressure difference between the airways inlet and the intrapleural fluid
\vec{u}	Velocity of the carrying fluid
A_c	Cross sectional area of the capillary
A_i	Cross sectional area of the branch
A_{ca}	Capillary-alveolus contact area
A_{in}	Inlet area cross sectional area of the bronchiole
c	Species concentration
D	Branch diameter
D_c	Diameter capillary
DSV	Dead space volume
FRC	Functional residual capacity
k_H^{cc}	Henry's constant
L	Branch length
N	Total number of number of alveoli
N_i	Number of branches in generation i
$P_b(\xi, t)$	species partial pressure in the blood along the capillary
$p_{ip,max}$	Maximum intrapleural pressure
$p_{ip,min}$	Manimum intrapleural pressure
$Q(t)$	Volume flow rate predicted by the mechanical model
R	Universal ideal gas constant

T	Temperature
U_b	Blood speed in capillaries
W	contact area between the capillary and the alveolar membrane, per unit length of the capillary
C	Compliance of the lung tissue
D	Mixing coefficient of the species in the carrying fluid.
$D_{\bullet,air}$	Mass diffusion coefficient of the species in air
$D_{\bullet,water}$	Species diffusion coefficient in the membrane
\mathcal{R}	Airways resistance
$\bar{q}_{a \rightarrow b}$	Mean species flux from the alveolar space to the blood
$C_a(t)$	Mean concentration of the species in the alveolus

Chapter 1

Introduction

A previous lung model was built, at AUB, to investigate blood oxygenation in preterm infants treated by Bubble-Nasal CPAP. The model covers relations between volume and pressure in the lung tissue (lung mechanics), oxygen distribution in the airways and alveoli during respiration, and oxygen uptake by the pulmonary capillaries (oxygenation). This model was then improved to have a generalized breathing simulator that is able to monitor the breathing of a human being and the ways it can be altered due to various lung abnormalities and corresponding treatments. This was achieved by: (i) Estimating lung parameters such as number of alveoli, blood volume entering the lungs, tidal volume, and many more, over a span of age, height, and body weight to generalize the model from preterm infants to any human being. (ii) Including carbon dioxide in the model. From the onset of inspiration, until gas exchange, then expiration, carbon dioxide distribution was solved in parallel with oxygen distribution for a more realistic model. (iii) Improving gas exchange across the alveolar-capillary membrane by integrating oxygen and carbon dioxide dissociation curves. Oxygen and carbon dioxide concentrations and partial pressures were interrelated during the exchange through these curves. The current work takes this model as a starting point and improves it by:

1. Updating the model into a more realistic one that mimics the several generations of the airways, which has a great impact on gas transport. The airways were previously modeled as a bundle of parallel tubes of equivalent airway resistance.
2. Validating and adding new reported measurements into the submodels such as:
 - Adding new reported measurements for the lung volumes and updating the code with various models for deadspace, tidal volume and Functional residual capacity, which provides the user with many options when using the GUI tool.

- Adding new estimates for the number of alveoli reported in literatures that used more accurate counting techniques, and gathering additional data related to the size of the alveolus in adults and infants.
 - Checking if all parameters related to capillary are reported in literature such as capillary diameter, blood transit time in the capillary, capillary to alveolus ratio, etc.
3. Integrating the previous model into a java environment through an automated flow. We used java for building a GUI tool that facilitates the model's usage, this tool takes as input the general data of the patient like age, gender, percentile, etc. and gives as output the height and mass of the patient using growth charts for both males and females from the age of few days till the age of 20 . Also it takes as input the number of generations to generate the network model and display the created airways' measurements and properties. Furthermore, it allows the user to track species transport starting from the mouth and ending up in the blood through dynamic plots.

Then the final version of this model was used to carry out assessment of airways geometric models based on gases transport to the blood. Geometric structure of airways controls, to a large extent, transport of gases and aerosols in the respiratory system. These airways form a complex branching network, whose mathematical descriptions (e.g., connectivity, an airway's length-to-diameter ratio, etc.) underpin most quantitative studies in dosimetry [16, 17] and in respiratory and obstructive diseases [18, 19]. Mathematical models of the bronchial tree in the human lung typically postulate a scaling law that relates the (generation-averaged) characteristics (diameter, length and branching angle) of each bronchial generation to those of the previous and successive generations.

There is a general consensus that the human bronchial tree forms a bifurcating network [19, 20]. The nature of bifurcations appears to be settled as well: while earlier and/or highly idealized models assume bifurcation symmetry [17, 21, 22], more recent investigations allow bifurcations in bronchial trees to be asymmetric [19, 20, 23]. Finally, guided by morphometric data [24, 25, 26], most (if not all) network models assume certain geometric properties scale across generations of the bronchial tree. Examples of such scaling laws are Weibel's [21] and Horsfield's [11] models of bifurcation. The former posits that, in symmetrically bifurcating trees, a branch size S (e.g., its length and diameter) scales with the branching order n as $S(n) = S(0)\alpha^n$; in other words, the knowledge of the trachea size, $S(n = 0)$, and the scaling factor $\alpha < 1$ is sufficient to estimate the branch size in any generation n of the bronchial tree. The latter uses the same form of scaling law, $S(m) = S(0)\beta^m$, but groups the airways in order to account for the network asymmetry and starts the counting from the periphery upward, such that $S(m = 0)$ is the smallest size and $\beta > 1$.

The parameters in these, and more evolved [27, 2], models are obtained by op-

timizing the bronchial tree's function. There is considerable debate about which specific cost function of the lung is to be optimized. It has been argued that the bronchial trees have evolved in a way that their bronchus' length-to-diameter ratio minimizes the total pressure loss across the bronchi [22], that their asymmetrically bifurcating structure minimizes either dissipation of frictional energy [28] or a linear combination of the tree's resistance and volume [29], maximizes the volumetric flow rate [14], etc. Natural in- and intra-species variability add a certain degree of randomness to the bronchial tree's structure [29], making it all but impossible to determine which cost function is "correct".

In lieu of such a verification, predictions of mathematical models of air flow in the bronchial networks are compared with relevant observations. We start by providing a quantitative assessment of the existing network and gas flow models' ability to predict observable geometric and mechanistic characteristics, such as network resistance, dead space volume, and path length. The choice of these metrics is justified by the availability of their (relatively) high-fidelity experimental measurements. Then we present a model of dynamic transport of oxygen and carbon dioxide along the airways, in the alveoli, across the alveolar membrane, and along the pulmonary blood capillaries. The model also accounts for the exchange of these two gases with blood in the capillaries, as well as age, gender and other in-species characteristics. Finally, our model's predictions are compared with corresponding observations, providing an additional venue to assess the validity of the existing models of the lung's bronchial tree. We are not aware of any other comparison involving blood gas transport.

Chapter 2

Review of the tracheobronchial tree

Available data on the (generation-averaged) length $L(n)$ and diameter $D(n)$ of individual bronchus in the n th generation ($n = 1, \dots, 24$) of the human bronchial tree are collated in Tables 2.1 and 2.2, and presented graphically in Figure 2.1. These data are separated by age, such that Table 2.1 and the top row in Figure 2.1 present data for human adults, while Table 2.2 and the bottom row in Figure 2.1 are for human infants. These data served to inform multiple models of the human bronchial tree, six of which are described below.

Table 2.1: Length (L) and diameter (D), both in mm, of the n th bronchi generation, predicted with tree models A–G for human adults. Model A [2] infers $L \sim n^{-1.38}$ and $D \sim n^{-1.26}$ from data; Model B [10] $L \sim \exp(-0.92n)$ and $D \sim \exp(-0.39n)$ for $n \leq 3$, and $L \sim \exp(-0.17n)$ and $D \sim \exp(-0.29n+0.01n^2)$ for $n > 3$; Model D [11] $D \sim a^{25-n}$ with $a > 1$ varying between three groups of bronchi characterized by three intervals of n ; and Model E [12] identifying a linear relation, for each generation, between bronchi’s length & diameter and human height H , $L \sim H$ and $D \sim H$. The remaining tree models, C [13], F [1] and G [14], fit no curves to the data reported therein.

n	A [2]		B [10]		C [13]		D [11]		E [12]		F [1]		G [14]	
	L	D	L	D	L	D	L	D	L	D	L	D	L	D
1	120	18	120	18	100	16	100	16	89	18.2	120	16.8	120	20
2	46.1	7.5	47.8	12.21	50	12	40	12	38.3	13.0	47.8	11.4	42.2	18
3	26.4	4.5	19.1	8.3	22	11	26	10.3	14.7	9.0	19.1	7.1	30.3	13
4	17.7	3.1	7.6	5.6	11	8	18	8.9	10.5	6.7	7.6	4.4	23.4	9.4
5	13.0	2.4	12.7	4.5	10.5	7.3	14	7.7	8.1	4.0	12.7	3.4	18.4	7.2
6	10.2	1.9	10.7	3.5	11.3	5.9	11	6.6	6.91	3.16	10.7	2.7	14.6	5.7
7	8.2	1.6	9.0	2.8	11.3	5.9	10	5.7	5.0	2.6	9.0	2.1	10.7	4.5
8	6.8	1.3	7.6	2.3	9.7	5.4	10	4.9	3.6	1.7	7.6	1.7	9.8	3.6
9	5.8	1.1	6.4	1.9	10.8	4.3	10	4.2	2.9	1.2	6.4	1.4	7.8	3
10	5	1.0	5.4	1.5	9.5	3.5	10	3.5	2.9	1.0	5.4	1.1	6.5	2.4
11	4.4	0.9	4.6	1.3	8.6	3.5	9.6	3.3	2.5	0.8	4.6	1.0	5.3	2
12	3.9	0.8	3.9	1.1	9.9	3.1	9.1	3.1	2.3	0.6	3.9	0.8	4.3	1.6
13	3.5	0.7	3.3	1.0	8	2.9	8.6	2.9	2.1	0.6	3.3	0.7	3.6	1.3
14	3.1	0.7	2.7	0.8	9.2	2.8	8.2	2.8	1.9	0.6	2.7	0.6	2.8	1.1
15	2.9	0.6	2.3	0.7	8.2	2.7	7.8	2.6	1.7	0.5	2.3	0.5	2.5	0.9
16	2.6	0.6	2.0	0.7	8.1	2.5	7.4	2.4	1.6	0.5	2.0	0.5	2.0	0.7
17	2.4	0.5	1.7	0.6	7.7	2.4	7	2.3			1.7	0.4	1.6	0.6
18	2.2	0.5	1.4	0.5	6.4	2.2	6.7	2.2			1.4	0.4	0.8	0.5
19	2.1	0.4	1.2	0.5	6.3	2	6.3	2			1.2	0.4	0.8	0.7
20	1.9	0.4	1.0	0.5	5.2	1.8	5.7	1.8			1.0	0.3	1	0.8
21	1.8	0.4	0.8	0.5	4.8	1.6	5	1.5			0.8	0.3	1	0.4
22	1.7	0.4	0.7	0.4	4.2	1.4	4.4	1.3			0.7	0.3	1	0.4
23	1.6	0.4	0.6	0.4	3.6	1.1	3.9	1.1			0.6	0.3	0.8	0.4
24	1.5	0.3	0.5	0.4	3.1	1.0	3.5	0.9			0.5	0.3	0.6	0.4
25							3.1	0.8						

Model A. The fractal lung model [27, 2] assigns a probabilistic density function to scaling factors for the dimensions of parent and daughter bronchi and employs the renormalization group theory to account for the heterogeneity in the asymmetric airway branching. The model predicts the average dimensions (diameter, length, and volume) of the airways to obey power laws in the generation number n (see the caption of Table 2.1), with the model parameters inferred by fitting the model to the data from [21, 24].

Model B. The symmetrically bifurcating model of Weibel [21, 26] predicts the diameter and length of a bronchus to follow an exponential law in the generation number n (see the caption of Table 2.1). The model was inferred from, and parameterized by, a complete set of measurements of the first six generations

($1 \leq n \leq 7$) of airways' diameters and lengths, some measurements from generations $8 \leq n \leq 11$, and morphometric estimates of the lengths and diameters of respiratory bronchioles and alveolar airways ($n \geq 12$).

Model C. This model also assumes a fractal structure of the branching, with a self-similarity distribution that is preserved up to the 24th generation. The dimensions of the airways are inferred from prior observations [30, 31, 32, 33, 22, 21].

Model D. The asymmetric bifurcation model [11, 34] orders airways by their relation to the periphery, as opposed to the trachea, groups them by similar size, and subdivides them into zones according to their degree of asymmetry. This ensures that the airways of the same order are more uniform in size than the airways of the same generation in model B [21, 26]. Measurements of the complete human bronchial tree [11, 34] are used to linearly correlate bronchi length L with their diameter D .

Table 2.2: Length (L) and diameter (D), both in mm, of the n th bronchi generation, predicted with the tree models A [2], E [12], and H [15] for human infants.

n	A [2]		E [12]		H [15]	
	L	D	L	D	L	D
1	26.5	5.69	26.5	5.69	26.5	3.28
2	11.06	2.19	15.79	4.34	15.79	2.8
3	6.64	1.25	5.96	3.28	5.96	1.91
4	4.62	0.84	3.89	2.59	3.89	1.51
5	3.49	0.62	3.71	1.85	3.71	1.47
6	2.77	0.48	2.78	1.41	2.78	1.21
7	2.28	0.39	2.22	1.14	2.22	1
8	1.93	0.32	1.98	0.85	1.98	0.89
9	1.66	0.27	1.92	0.7	1.92	0.87
10	1.46	0.24	1.75	0.64	1.75	0.78
11	1.29	0.21	1.64	0.58	1.64	0.72
12	1.16	0.18	1.57	0.51	1.57	0.68
13	1.05	0.17	1.5	0.5	1.5	0.64
14	0.95	0.15	1.43	0.47	1.43	0.6
15	0.87	0.14	1.36	0.45	1.36	0.55
16			1.3	0.43	1.3	0.51

Model E. The model [24, 12] accounts for the bronchi orientation to gravity and angles at branching points, and establishes linear relationships between a bronchus' length/diameter and the body height. This information is absent in

both symmetric [21, 26] and asymmetric [11, 34] models. The model is derived from a set of observations (casts) collected in humans, dogs, rats and hamsters. This data set seems to support the notion that airway branching in humans is overall symmetric.

Model F. The symmetrical dichotomous branching model [1] generalizes the model B [21, 26] by incorporating the mechanisms involved in airway narrowing due to shortening of the smooth muscle.

Model G. The asymmetric model [14] postulates that the bronchial tree possesses an optimal topology that serves to provide a best physiological function. The chosen function is the lung's ability to move the respiratory gases. The subsequent studies, some of which are referenced in the introduction, suggest a number of alternative lung functions as optimization target.

Model H. The asymmetric model [15] provides a statistical representation of the tracheobronchial tree. The model consists of generation-specific probability density functions for airway diameters, airway lengths, branching angles, and gravity angles. In each generation, the vessel diameter is related to its length $D = 2.115 \ln L + 0.267$.

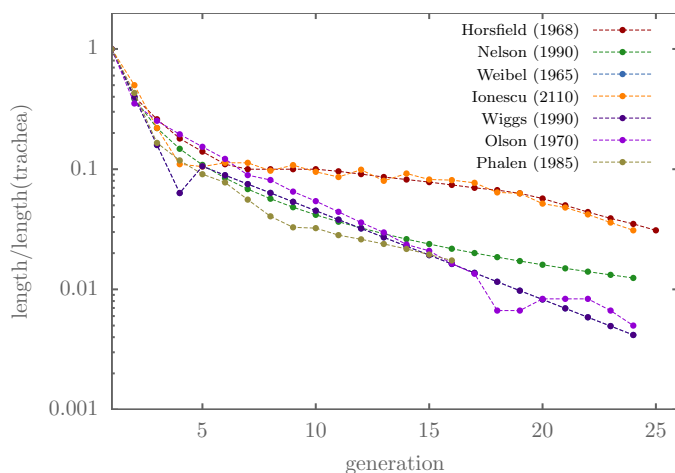


Figure 2.1: Airways generation length, normalized by the length of the trachea, vs the generation order for adults.

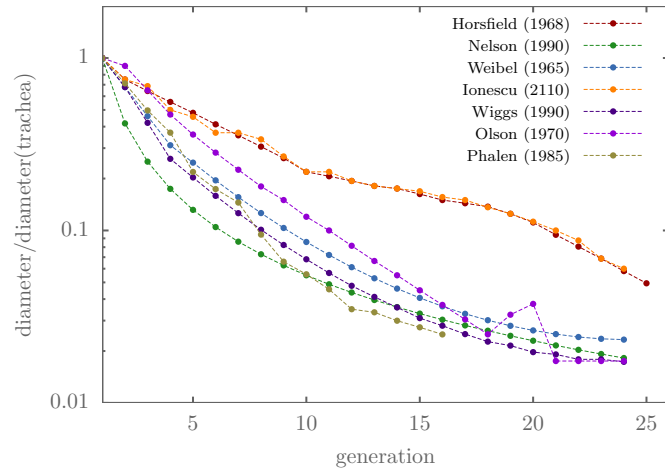


Figure 2.2: Airways generation diameter, normalized by the diameter of the trachea, vs the generation order for adults.

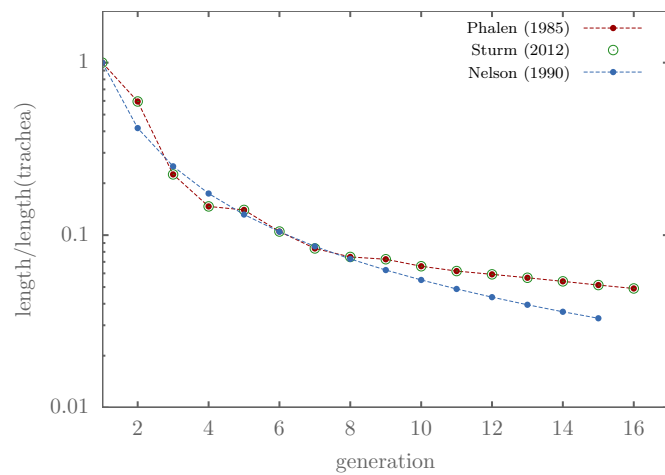


Figure 2.3: Airways generation length, normalized by the length of the trachea, vs the generation order for infants.

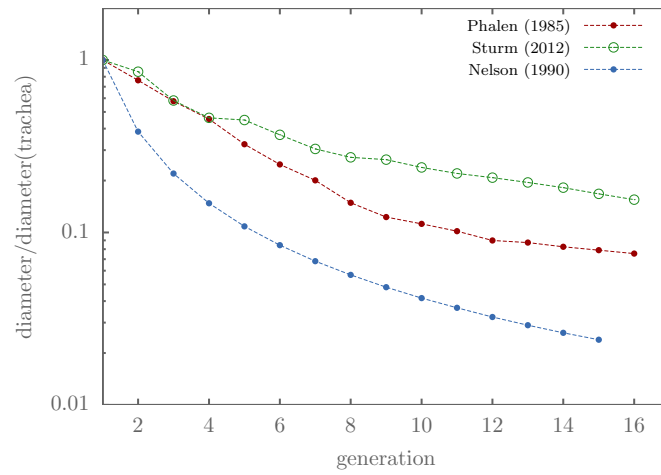


Figure 2.4: Airways generation diameter, normalized by the diameter of the trachea, vs the generation order for infants.

So far no one has assessed the geometric models based on blood gas transport, in our work each of the previous presented models was evaluated based on how gases are distributed in capillary and alveolus versus time and space.

Chapter 3

Our model

3.1 The mechanical model

A circuit representation of a general mechanical model of the airways is shown in figure 3.1-a. In this model, each branch is represented as a resistance in series with an inductance, and a shunt capacitance, modeling the effects of friction, inertia, and storage, respectively. Note that the capacitive behavior arises when the channel wall is compliant.

[h!]

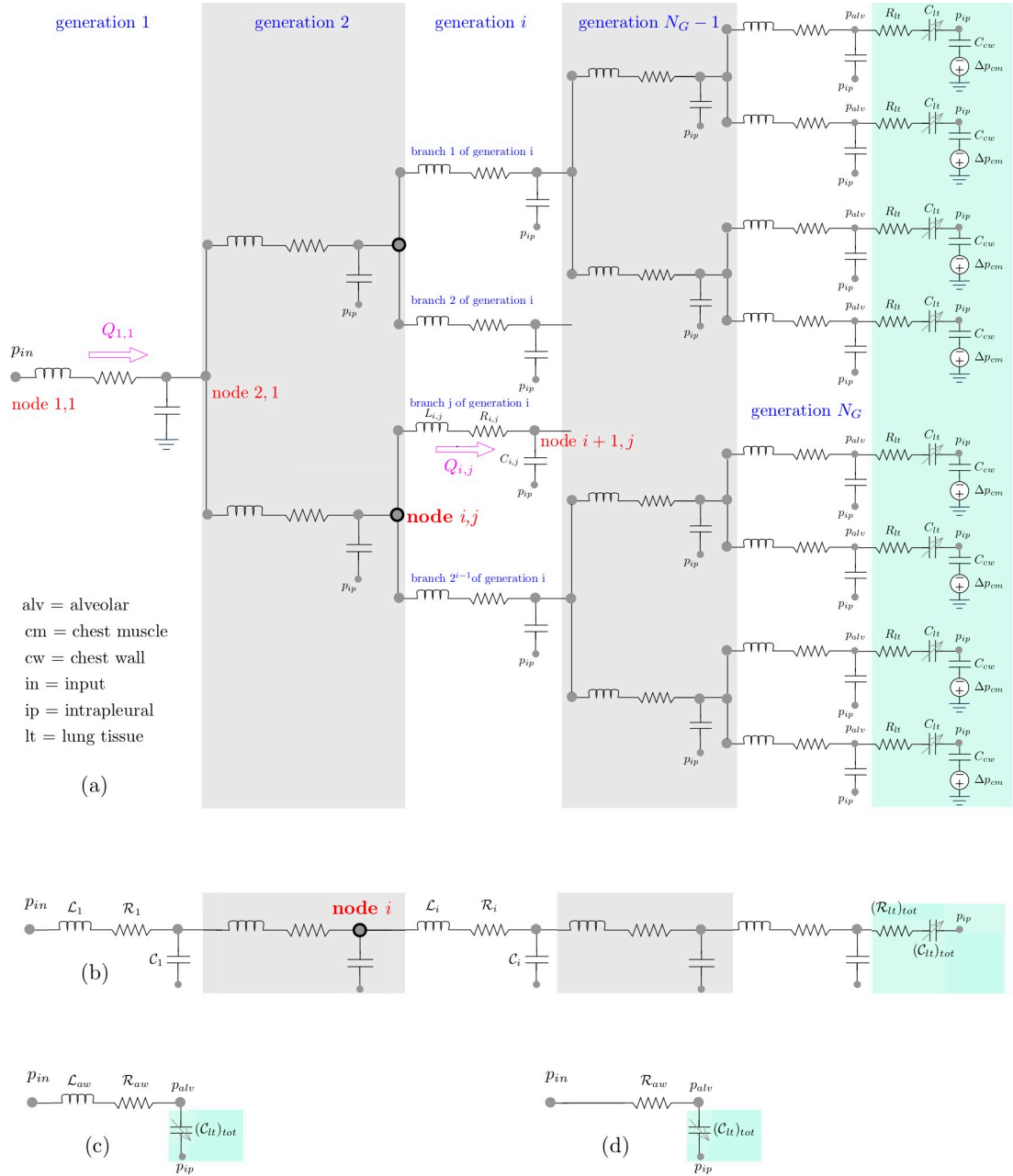


Figure 3.1: (a) circuit representation of a general airways mechanical model. (b) a simplified model.

If the channels belonging to a each generation are identical and if the lung

tissue resistance and compliance are uniformly distributed over the alveoli, then all the nodes in a branch have the same potential (pressure) as the corresponding nodes in all the branches belonging to the same generation. In this case, the airways can be collapsed into a circuit in series, as depicted in Figure 3.1-b, where nodes (i, j) , $j = 1..2^{i-1}$ of the circuit (a) are collapsed onto node i in the simplified circuit (b).

If the compliance of the channel wall is small, it can be approximated as rigid so that all capacitors C_i can be replaced by open circuits. This assumption is justified by the fact that the lung tissue compliance, associated with the expansion/contraction of the alveoli is much larger than that associated with expansion/contraction of the airways channels [35]; i.e. $(C_{lt})_{tot} \gg C_i$. The circuit of Figure 3.1-b can then be further simplified into that shown in Figure 3.1-c, where $\mathcal{L}_{aw} = \sum_i \mathcal{L}_i$ and $\mathcal{R}_{aw} = \sum_i \mathcal{R}_i$. The circuit model (c) also neglects the tissue resistance, which is typically much smaller than the airways resistance [36], i.e. $(\mathcal{R}_{lt})_{tot} \ll \mathcal{R}_{aw}$.

If, additionally, inertia effects are small, the inertance can be neglected and the lung mechanical model is represented by the simple $R - C$ circuit in Figure 3.1-d.

For the $R - C$ model of figure 3.1-d, the relationship between an applied pressure signal and the lung volume is expressed as:

$$\Delta p = \mathcal{R} \frac{dV}{dt} + \frac{V - V_0^*}{\mathcal{C}} \quad (3.1)$$

where Δp is the pressure difference between the airways inlet and the intrapleural fluid, \mathcal{C} is the compliance of the lung tissue, and \mathcal{R} is the airways resistance. The initial total alveolar volume, V_0^* , is obtained as follows. At the beginning of inspiration (end of expiration), the $\Delta p - V$ behavior is nearly static, the intrapleural pressure is maximum; $p_{ip} = p_{ip,max}$, and the total alveolar volume is equal to the difference between the functional residual capacity and the dead space; $FRC - DSV$. When the airways inlet gauge pressure is 0, as in normal unassisted breathing, we get $V_0^* = (FRC - DSV) - \mathcal{C}|p_{ip,max}|$. For the purpose of comparing the airways geometries in terms of gases transport, the initial alveolar radius R_{a0} is chosen to be $100 \mu m$ for adults [37] and $20 \mu m$ for infants [38]. When the airways inlet gauge pressure is 0, as in normal unassisted breathing, we get $V_0^* = \frac{4N_a\pi R_{a0}^3}{3}$, where N_a is the total number of alveoli.

For normal breathing of an adult, typical values are $\mathcal{R} = 0.56 \text{ cmH}_2\text{O.s/l}$, $\mathcal{C} = 93.66 \text{ ml/cmH}_2\text{O}$, $FRC = 3228.27 \text{ ml}$, $DSV = 830 \text{ ml}$, $p_{ip,min} = -10 \text{ cmH}_2\text{O}$ and $p_{ip,max} = -5 \text{ cmH}_2\text{O}$. For a breathing frequency of 0.25 Hz (15 bpm) and inspiration to expiration ratio of 0.5, the pressure signal and the total alveolar volume response are plotted against time in Figure 3.2. The corresponding lung hysteresis curve is shown in Figure 3.3.

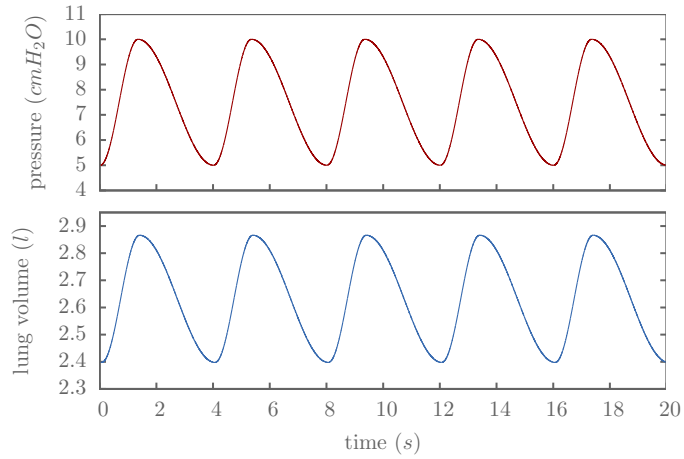


Figure 3.2: Time variation of the pressure signal and the total alveolar volume under normal breathing conditions for an adult.

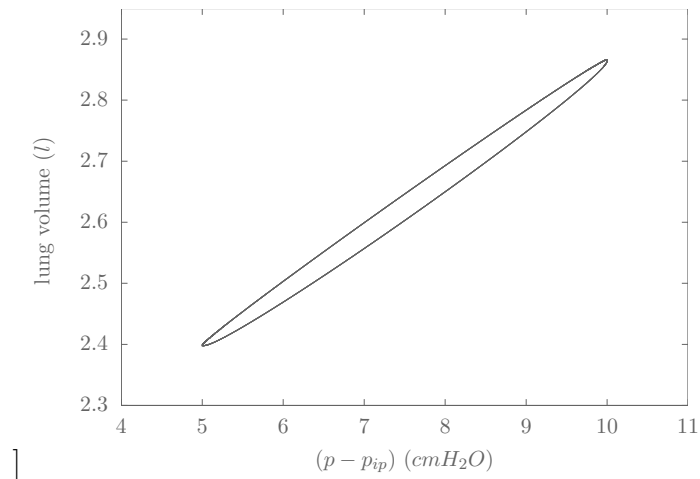


Figure 3.3: $\Delta p - V$ curve of the lung hysteresis.

3.2 The species transport model

The equation governing the species transport

$$\frac{\partial c}{\partial t} + \vec{u} \cdot \nabla c = \mathcal{D} \nabla^2 c \quad (3.2)$$

where c is the species concentration, \vec{u} is the velocity of the carrying fluid, and \mathcal{D} is the mixing coefficient of the species in the carrying fluid.

3.2.1 Gas transport in the airways

For each branch i of constant diameter D_i , we assume the flow to be axisymmetric and parallel, so that

$$\frac{\partial c}{\partial t} + u \frac{\partial c}{\partial x} = \mathcal{D} \left(\frac{\partial^2 c}{\partial x^2} + \frac{1}{r} \frac{\partial}{\partial r} \left(r \frac{\partial c}{\partial r} \right) \right) \quad (3.3)$$

Integrating over the cross sectional area, and noting that the radial flux of c is zero at $r = 0$ and $r = D_i/2$, we get

$$\frac{\partial C}{\partial t} + \frac{4}{\pi D_i^2} \int_0^{D_i/2} u \frac{\partial c}{\partial x} 2\pi r dt = \mathcal{D} \frac{\partial^2 C}{\partial x^2} \quad (3.4)$$

where $C(x, t) = \frac{4}{\pi D_i^2} \int_0^{D_i/2} c 2\pi r dt$.

Our model assumes that the gases are well mixed in the plane of the channel cross section.

Assuming that the gases are well mixed in the plane of the channel cross section, the transport of gases in an airway channel is governed by

$$\frac{\partial C_{aw}}{\partial t} + U_i(t) \frac{\partial C_{aw}}{\partial x} = \mathcal{D} \frac{\partial^2 C_{aw}}{\partial x^2} \quad (3.5)$$

where $C_{aw}(x, t)$ denotes the mean concentration of the gas (O_2 or CO_2) at position x and time t . Note that the mean flow speed is generation dependent. To conserve mass, the mean flow speed in a channel belonging to generation i is

$$U_i(t) = \frac{Q(t)}{N_i A_i} \quad (3.6)$$

where $Q(t)$ is the volume flow rate predicted by the mechanical model, $N_i = 2^{i-1}$ is the number of branches in generation i , assuming dichotomous branching, and $A_i = \pi D_i^2/4$ is the cross sectional area of the branch, as depicted in Figure 3.4.

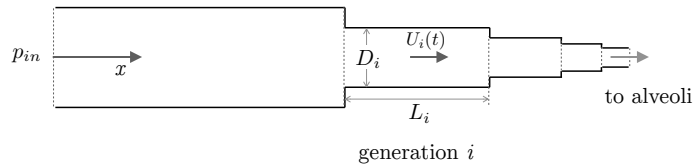


Figure 3.4: Species transport in the airways.

3.2.2 Gas transport in the alveoli

The alveolus is the smallest element of the respiratory system where gases are exchanged across the alveolar membrane between the air in the alveolar space

and the blood in the capillaries. As depicted in Figure 3.5, each terminal airways branch (bronchiole) is connected to $\frac{N_a}{2^{N_G-1}}$ alveoli, where N_a is the total number of alveoli and N_G is the number of airways generations. Dependence of the total number of alveoli on age and lung volume is presented in of section A.4, where data from different sources are plotted in Figures A.8, A.9, A.10. Our model, which covers the whole age range, is a fit that favors more recent data. For an adult, the number of alveoli per bronchiole is approximately 60, assuming 500 million alveoli and airways composed of 24 generations.

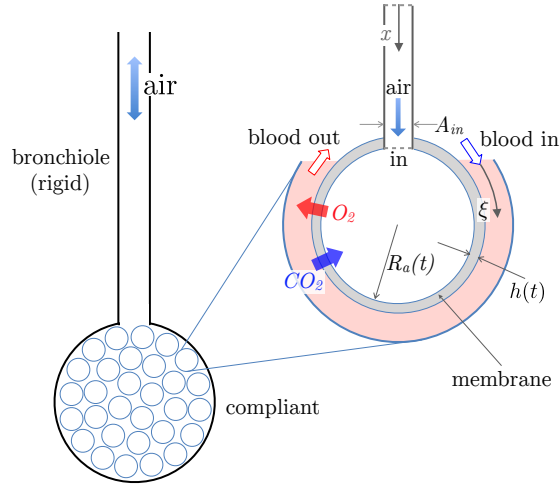


Figure 3.5: Each terminal branch is connected to a number of alveoli. Our model assumes that the bronchiole is connected to the center of each compliant spherical alveolus.

The alveoli are considered to be spherically-shaped compliant elements that change their volume with time according to

$$\frac{dV_{at}(t)}{dt} = Q(t), \quad V_{at}(t) = N_a V_a(t), \quad V_a(t) = \frac{4\pi R_a^3(t)}{3} \quad (3.7)$$

Note that at the end of expiration, the total alveolar volume, V_{at} , is equal to

$$V_{at}^{(0)} = FRC - DS \quad (3.8)$$

where FRC and DS are respectively, the functional residual capacity and the dead space. Correlations for FRC and DS , based on data from numerous sources, are presented in Figures A.12 and A.14 of section A.5.2 and A.5.3 respectively. Decomposition of the lung volume into FRC , DS and V_a is plotted versus age in Figure A.13.

Taking the alveolar space shown in Figure 3.5 as a control volume, the balance of species transport yields

$$\frac{d(C_a(t)V_a(t))}{dt} = Q_{in}C_{in} - A_{ca}\bar{q}_{a \rightarrow b} - \mathcal{D}_{\bullet,air}A_{in} \left. \frac{\partial C(x,t)}{\partial x} \right|_{in} \quad (3.9)$$

where C_a is the mean concentration of the species in the alveolar space, $Q_{in} = Q(t)/N_a$, $\bar{q}_{a \rightarrow b}$ is the mean species flux from the alveolar space to the blood, $\mathcal{D}_{\bullet,air}$ is the mass diffusion coefficient of the species in air. C_{in} and $\left. \frac{\partial C(x,t)}{\partial x} \right|_{in}$ are the species concentration and its x -gradient at the inlet to the alveolus. A_{in} and A_{ca} are respectively the inlet area cross sectional area of the bronchiole and the capillary-alveolus contact area.

3.2.3 Gas transport in the pulmonary membrane

Exchange of gases between the alveolar air and the blood circulating in the surrounding capillaries occurs by diffusion through a $\sim 0.6 \mu\text{m}$ thick pulmonary membrane[39]. Diffusive transport across the membrane is driven by a difference in partial pressure between the blood side and the alveolar side. Typically oxygen partial pressure is higher in the alveolus while carbon dioxide partial pressure is higher on the blood side so that oxygen diffuses from the alveoli to the capillaries and carbon dioxide diffuses from the capillaries to the alveoli, as depicted in Figure 3.5. Since the radius of the alveolus is two orders of magnitude larger than the membrane thickness, the membrane is assumed to be locally planar, so that the molar species concentration, C , in the membrane is governed by

$$\frac{\partial C}{\partial t} = \mathcal{D}_{\bullet,water} \frac{\partial^2 C}{\partial r^2} \quad (3.10)$$

where $\mathcal{D}_{\bullet,water}$ is the species diffusion coefficient in the membrane, which is modeled as a body of water. Noting that the diffusion time scale ($h_0^2/\mathcal{D}_{\bullet,water} \sim 1 \text{ms}$ for O_2 and CO_2) is much smaller than the respiration period (1.5 - 4 s), we assume diffusion through the membrane to be quasi-steady so that the species flux in the membrane is uniform

$$q_{a \rightarrow b}(\xi, t) = \frac{\mathcal{D}_{\bullet,water}}{k_H^{cc}} \frac{C_a(t) - \frac{P_b(\xi, t)}{RT}}{h(t)} \quad (3.11)$$

where $C_a(t)$ is the mean concentration of the species in the alveolus, $P_b(\xi, t)$ is the species partial pressure in the blood along the capillary, k_H^{cc} is Henry's constant, R is universal ideal gas constant, and T is the temperature. Note that, on the blood side, P and C are related by the dissociation curves, presented in the next section.

The alveolar membrane is viscoelastic and respond to any change in alveolar pressure. By conserving the volume of the membrane, V_{am} , its thickness, $h(t)$, varies in time according to

$$h(t) = \sqrt[3]{\frac{3}{4\pi} \left[V_{am} + \frac{4}{3}\pi R_a^3(t) \right]} - R_a(t) \quad (3.12)$$

3.2.4 Gas transport in the blood

Each alveolus is surrounded by a number of capillaries that form a sheet of blood flow to promote the exchange of oxygen and carbon dioxide. Of the oxygen captured by the blood, $\sim 97\%$ is bound to the hemoglobin in the red blood cells that flow in a single file in the capillary. The concentration of oxygen bound to hemoglobin can be related to its partial pressure in blood through the empirical dissociation curve. Several effects such as blood acidity and chemical composition may alter the saturation capacity of hemoglobin through a leftward or rightward shift in the dissociation curve. Carbon dioxide can be transported in blood in three different ways: dissolved in the plasma, as bicarbonate ions, and forming the carbamino-hemoglobin complex. Interactions between oxygen and carbon dioxide with hemoglobin through chemical reactions promote the delivery of oxygen to the blood and expulsion of carbon dioxide to the alveoli [40]. As in [41], our blood perfusion model treats the blood in pulmonary capillaries as a uniform homogeneous phase (masking the discrete constituents: plasma and erythrocytes). The model also assumes equilibrium conditions for the reactions thus allowing use of the empirical dissociation curves to relate the partial pressure to the species concentration. Denoting U_b to be the speed of blood along the capillary, the concentrations of O_2 and CO_2 along the capillary are governed by

$$\frac{\partial O_{2,b}}{\partial t} + U_b \frac{\partial O_{2,b}}{\partial \xi} = \frac{W}{A_{cap}} q_{O_2,a \rightarrow b} \quad (3.13)$$

$$\frac{\partial CO_{2,b}}{\partial t} + U_b \frac{\partial CO_{2,b}}{\partial \xi} = \frac{W}{A_{cap}} q_{CO_2,a \rightarrow b} \quad (3.14)$$

where A_c is the cross sectional area of the capillary and W is the contact area between the capillary and the alveolar membrane, per unit length of the capillary. The diameter of the capillary, D_c , is taken to be equal to $8 \mu m$; the size of a red blood cell. Each alveolus is surrounded by several capillaries in which the red blood cells travel at the blood speed U_b . Gas exchange between the alveolar space and the blood circulating in the surrounding capillaries is a function of the blood speed in the capillaries, the contact area between an alveolus and the surrounding capillaries, and the capillaries distribution.

The capillaries blood flow model takes as an input the percent contact area between the alveoli and the capillaries (β), and the residence (transit) time of the blood in the pulmonary capillaries, (t_r). A typical value of $t_r \approx 1$ sec [42]. An upper bound on the blood volume in the capillaries, $V_{b,max}$, is determined by assuming that each alveolus is surrounded by a spherical shell of thickness equal to the diameter of the capillary:

$$V_{b,max} = N_a 4\pi R_{a0}^2 D_c \quad (3.15)$$

The actual blood volume in the pulmonary capillaries then based on the

$$V_b = \beta V_{b,max} \quad (3.16)$$

From the blood volume and the resident time, the volume flow rate of blood in the pulmonary capillaries is

$$\dot{V}_b = \frac{V_b}{t_r} \quad (3.17)$$

The capillaries blood flow rate per alveolus is:

$$\dot{V}_{b,a} = \frac{\dot{V}_b}{N_a} \quad (3.18)$$

The capillary distribution model assumes that a single capillary extends over half of the alveolar perimeter ($L_c = \pi R_{a,0}$). The number of capillaries per alveolus is

$$N_{c,a} = \frac{\frac{V_b}{N_a}}{A_c L_c} \quad (3.19)$$

where A_c is the cross sectional area of the capillary; $A_c = \frac{\pi D_c^2}{4}$. Then, the speed of blood in a single capillary is

$$U_b = \frac{\dot{V}_{b,a}}{N_{c,a} A_c} \quad (3.20)$$

Equations (3.13) and (3.14) are coupled through the interdependence between O_2 and CO_2 , imposed by the blood chemistry, as described next. The oxygen-hemoglobin dissociation curve (ODC) relates the saturation of hemoglobin with oxygen to the oxygen partial pressure in the blood [43]. The curve also captures the explicit dependence of the oxygen partial pressure on the carbon dioxide partial pressure and pH. The ODC relation [44], derived from a kinetic study of the several chemical reactions between the respiratory gases and hemoglobin, is written as follows:

$$S = 100 \frac{K_0 P_{O_{2,b}}^n}{1 + K_0 P_{O_{2,b}}^n} \quad (3.21)$$

$$K_0 = \frac{(1 + 10^{-pH} K_2 + \frac{\gamma K_6 P_{CO_{2,b}}}{10^{-pH}}) K 10^{lpH}}{1 + 10^{-pH} K_1 + \frac{\gamma K_5 P_{CO_{2,b}}}{10^{-pH}}} \quad (3.22)$$

S is the hemoglobin saturation in %, $P_{O_{2,b}}$ and $P_{CO_{2,b}}$ are the oxygen and carbon dioxide partial pressures respectively. $K_0, K_1, K_2, K_5, K_6, K, \gamma, l$ are constants determined by [44]. Note that The oxygen concentration can be obtained from S according to

$$S = 100 \frac{O_{2,b}}{O_{2,b|S=100\%}} \quad (3.23)$$

where the blood concentration at 100% saturation is $O_{2,b|S=100\%} = 201$ mL/L.

The carbon dioxide dissociation curve relates directly the carbon dioxide concentration to its partial pressure in the blood according to the following relation [45, 46]

$$CO_{2,b} = f(P_{CO_{2,b}}, P_{O_{2,b}}) = 462e^{0.00415P_{CO_{2,b}}} - 340e^{-0.0445P_{CO_{2,b}}} + 0.62(97.5 - S) \quad (3.24)$$

$CO_{2,b}$ is expressed in mL/L and S is the hemoglobin saturation with oxygen found in equation 3.21. The relation covers a wide range of carbon dioxide partial pressure (10 mmHg $< P_{CO_{2,b}} < 80$ mmHg).

Coupling between O_2 and CO_2 in the blood chemistry is responsible for the Bohr and Haldane effects. Bohr: as the partial pressure of CO_2 decreases, the hemoglobin saturation (and the O_2 concentration), for a given partial pressure of O_2 , increases. Haldane: as the hemoglobin saturation decreases (and the O_2 concentration), the CO_2 concentration, for a given partial pressure of CO_2 , increases. This coupling makes it impossible to solve for the distributions of O_2 and CO_2 independently. This coupling, captured by equations above, imposes a nonlinear constraint on the equations governing transport on gases in the blood.

The boundary condition of equations (3.13) and (3.14) at the inlet to the capillaries are chosen to be $(P_{O_{2,b}})_{in}=40$ mmHg and $(P_{CO_{2,b}})_{in}=46$ mmHg.

3.3 Numerical Implementation of the Model

The airways species transport model takes as input the means flow speeds U_i from the mechanical model, in additions to the channels dimensions L_i and D_i from the airways geometry model or measurements. Equation (3.5), governing species transport in the airways, is subject to a Dirichlet boundary condition at the inlet (to trachea) and to a mixed boundary condition at the outlet. Using equation (3.9) governing species balance in the alveolus, the mixed boundary condition at the airways outlet (inlet to alveoli) may be expressed as

$$Q_{in}C_{in} - \mathcal{D}_{\bullet,air}A_{in} \left. \frac{\partial C(x,t)}{\partial x} \right|_{in} = f(t) \quad (3.25)$$

where

$$f(t) = \frac{d(C_a(t)V_a(t))}{dt} + N_c W \int_0^{L_c} q_{a \rightarrow b}(\xi, t) d\xi \quad (3.26)$$

where N_c is the number of capillaries per alveolus and W is the capillary-alveolus contact area per unit length of the capillary. Note that $f(t)$ is dependent on the solution of the transport equations in the alveolar space, through the alveolar membrane, and in the blood, subject to the constraints imposed by the dissociation model. This coupled system of equations is numerically solved (from

$t - \Delta t$ to t) using two nested iteration loops. The inner loop adjust the species concentrations and partial pressures in the blood to satisfy the blood chemistry constraints and the outer loop matches $f(t)$, given in Equation(3.26), to the left hand side of equation (3.25).

We first describe our approach to solve gases transport in the blood, subject to the constraints imposed by the blood chemistry. The boundary conditions at the inlet to the capillary are fixed partial pressures of oxygen and carbon dioxide: $P_{O_{2,b}}=40$ mmHg and $P_{CO_{2,b}}=46$ mmHg. Noting that $dC_b/dt = \partial C_b/\partial t + U_b(t)\partial C_b/\partial x$ is the Lagrangian derivative measuring the change in the concentration per unit time of a particle moving with the flow, discretizing the capillary using a uniform grid of size $\Delta\xi = U_b\Delta t$ allows us to numerically solve Equations (3.13) and (3.14) for $C_b(\xi_i, t)$ using the second order integration scheme

$$C_b(\xi_i, t) - C_b(\xi_i - U_b\Delta t) = \frac{\Delta t}{2} (q_{a \rightarrow b}(\xi_i, t) + q_{a \rightarrow b}(\xi_i - U_b\Delta t, t - \Delta t)), \quad (3.27)$$

where $\xi_i = (i - 1/2)\Delta\xi, i = 1, \dots, L_c/\Delta\xi$. The concentration $O_{2,b}(\xi_i, t)$ and the associated hemoglobin saturation S are then capped to the maximum values ($O_{2,b|S=100\%}, 100\%$). This is followed by updating $P_{CO_{2,b}}(\xi_i, t)$ according to equation (3.24), followed by updating $K_0(\xi_i, t)$ and then $P_{O_{2,b}}(\xi_i, t)$ using equations (3.22) and (3.21), respectively. The updated values of the partial pressures are then used to update the fluxes $q_{a \rightarrow b}(\xi_i, t)$ for all cells along the capillary. The procedure is repeated until the solution converges.

Equations (3.5) are then numerically solved, using the mixed boundary condition (3.25) with $f(t)$ updated according to (3.26), to yield the species distribution in the airways, $C_{aw}(x, t)$. Values of $C_{aw}(x, t)$ and $\partial C_{aw}(x, t)/\partial x$ at the airways outlet (inlet to alveoli) are then used to update the concentrations in the alveolar space and the fluxes across the alveolar membrane. This will, in turn, enable us to update the gases concentrations in the blood along the capillaries using equation (3.27), subject to the blood dissociation constraints, as described above.

For spatial discretization along the airways channels, we choose the grid cell size to be $\Delta x = \min(\frac{L_k}{10}, \frac{L_{Ng}}{2})$. As for the capillaries, each is discretized into 100 elements along its length.

Chapter 4

Results

Assessment of the airways geometries of infants and adults is carried out by comparing with the two baseline cases presented in Table 4.1. These two baseline cases are a newborn and a 20 years old healthy males, with height and mass at the 50th percentile line of the growth charts. Other parameters, obtained from the data and relations of section A are also listed in the table.

Table 4.1: Baseline cases and model parameters values.

Parameter	infant	adult
Age (<i>yrs</i>)	0	20
Gender	male	male
Height (<i>cm</i>)	49.99	176.85
Mass (<i>kg</i>)	3.53	70.6
Frequency (<i>Hz</i>)	0.75	0.25
Tidal volume (<i>ml</i>)	21.7	468.3
Functional residual capacity (<i>ml</i>)	61.9	3228.27
Initial alveolar radius (μm)	20	100
Number of alveoli (<i>million</i>)	152	499
Minimum intrapleural Pressure (<i>cmH₂O</i>)	-10	-10
Maximum intrapleural Pressure (<i>cmH₂O</i>)	-5	-5
Compliance (<i>ml/cmH₂O</i>)	4.34	93.66

We assess the airways geometries by checking if the values of key physiological parameters, estimated using the airway geometries of tables 2.1 and 2.2, fall within independently measured values reported in the literature and summarized in section A. These parameters are: total resistance, dead space volume, total path length, and min and max mean partial pressure of oxygen and carbon dioxide in the capillaries. The results are summarized in Table 4.2. The measured values of the dead space for infants and adults are taken as averages of those reported

in Tables A.6 and A.5 respectively. The measured values of the resistance for infants and adults are taken as averages of those reported in Tables A.8 and A.7 respectively. Table 4.2 also lists the number of generations, length and diameter of the terminals branches.

Table 4.2: Comparison of the airways geometries in terms of dead space (DS), resistance (\mathcal{R}), total path length (L), time needed to reach saturation of oxygen in blood (T_r), mean oxygen partial pressure in blood ($\overline{P_{O_2}}$), and mean carbon dioxide partial pressure in blood ($\overline{P_{CO_2}}$). M: independently measured values. † corresponds to spatial averages along the capillary by assuming that P_{O_2} increases from 40 to 100 and P_{CO_2} decreases from 46 to 40 over one third of the capillary length. Partial pressures are in units of cmH_2O .

Model	DS	\mathcal{R}	L	T_r	$\overline{P_{O_2}}$		$\overline{P_{CO_2}}$	
	(mL)	($cmH_2O.s/L$)	(cm)	(sec)	(min)	(max)	(min)	(max)
adults								
[2]	2681.62	1.49	29.46	6	100.7	100.9	27	28.9
[10]	1656	0.184	27.28	1.3	100.4	100.8	17.3	22.4
[13]	77537	0.037	33.93	-	-	-	-	-
[11]	103141	0.037	34.53	-	-	-	-	-
[12]	71.07	0.357	19.4	21.4	96.2	101	42.9	45.4
[1]	830	0.56	27.27	1.3	100.5	100.9	21.8	28.7
[14]	1759	0.049	31.17	1.2	100.6	100.8	23.7	27.5
M	127-190	1.08-2.6	32	-	90†	90†	41†	41†
infants								
[2]	1.48	98.8	13.5	2	97.6	101.5	40.3	43
[12]	16.58	2.06	15.06	0.52	100.4	101.3	32	36.4
[15]	22.75	6.09	15.06	0.64	100.4	101.2	31	34.7
M	4.15-6.7	22.6-52	6.65	- 90†	90†	41†	41†	

Table 4.3: Comparison of the airways geometries in terms time constant (τ), number of airways generations (N_g), length and diameter of the last generation channels (L_{N_g} and D_{N_g}), the ratio of the airways inlets diameter per alveolus to the alveolar diameter, (R_{in}/R_{alv}), Reynolds number in the last generation ($\text{Re}_{N_g} = \frac{\rho \bar{u}_{N_g} D_{N_g}}{\mu}$), and Peclet number in the last generation ($\text{Pe}_{N_g} = \frac{L_{N_g} \bar{u}_{N_g}}{\mathcal{D}}$). ρ is the density, μ is the viscosity, \mathcal{D} is the diffusion coefficient of species in air, f . The mean speed is estimated based by assuming that the lung changes its volume by the tidal volume (TV) over half a breath period ($1/(2f)$), i.e. $\bar{u}_{N_g} = (2TV f)/2^{N_g-1}$.

Model	τ (<i>sec</i>)	N_g	L_{N_g} (<i>mm</i>)	D_{N_g} (<i>mm</i>)	R_{in}/R_{alv}	Re_{N_g}	Pe_{N_g}
adults							
[2]	0.14	24	1.49	0.328	0.045	0.01	0.04
[10]	0.017	24	0.501	0.418	0.073	0.01	0.01
[13]	0.003	24	3.1	0.96	0.387		
[11]	0.003	25	3.9	0.79	0.525		
[12]	0.033	16	1.55	0.454	0.0003	1.81	5.82
[1]	0.052	24	0.501	0.29	0.035	0.01	0.02
[14]	0.005	24	0.6	0.35	0.051	0.01	0.01
infants							
[2]	0.43	15	0.87	0.13	0.0011	0.54	3.15
[12]	0.009	16	0.429	0.3	0.012	0.28	0.76
[15]	0.026	16	0.429	0.507	0.035	0.23	0.53

Comparison is also carried out by inspecting, for each airway geometry, the oxygen and carbon dioxide partial pressures distribution along the capillaries every one eighth of a period over a whole period in the quasi-stationary state. In most cases, the quasi-stationary state was reached after ten breathing cycles. The time step used was 0.78 ms. The minimum and maximum values of the mean partial pressures of oxygen and carbon dioxide, listed in Table 4.2 for the various airways geometries, are obtained by averaging these distributions over the length of the capillary.

Since the time scale of diffusion across the alveolar membrane is proportional to the the square of the membrane thickness, it is very small compared to the time scales characterizing the other gases transport mechanisms. As such, gas exchange will occur very quickly between the alveolar space and blood, so that they remain close to each other as long as oxygen in the blood is below saturation level. This can be seen in Figure 4.1, where, when the blood is not saturated with oxygen, the partial pressure of oxygen in the alveolar space is close to but smaller than that in the blood indicating oxygen transport to the blood. It can

also be seen that the partial pressure of carbon dioxide in the blood is close to but larger than that in the alveolar space indicating transport to the alveolar space.

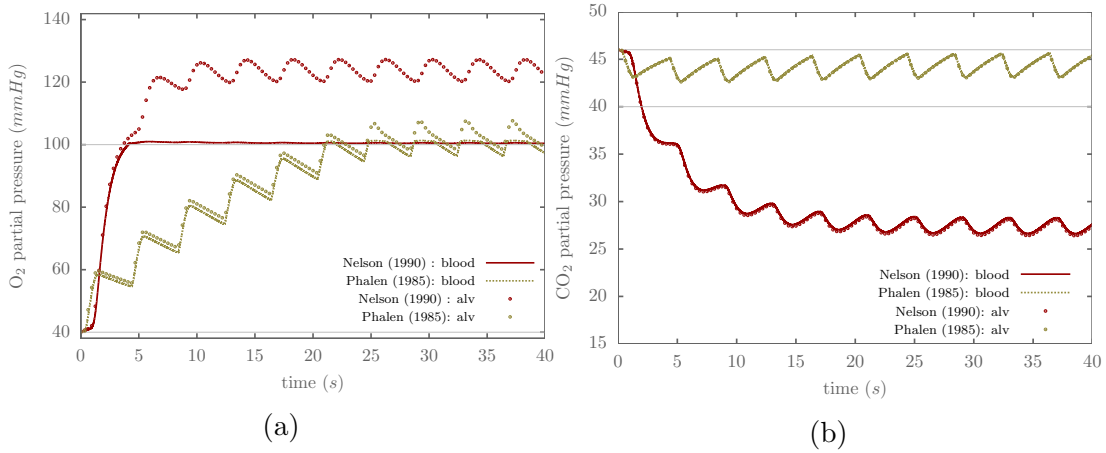


Figure 4.1: Comparison of the time variation of the mean partial pressure of Oxygen (left) and carbon dioxide (right) in the blood and in the alveolar space of adults for selected airways geometry models.

Figures 4.2a, 4.2b, 4.5a, 4.5b show the variation in time of the mean partial pressure of O_2 and CO_2 in the blood for adults and infants respectively, over 10 breathing cycles. We notice in figures 4.2a and 4.5a that oxygen is quicker to reach saturation in blood than carbon dioxide (Figures 4.2b and 4.5b). This is because while oxygen is only stored in the blood hemoglobin, carbon dioxide can be stored in the blood in different ways. Since carbon dioxide has a much higher solubility than oxygen, it can be transported easily in a dissolved state. More than 60% of carbon dioxide is stored in the bicarbonate ionic form [47], with 30% is stored in the hemoglobin and 7% in the plasma.

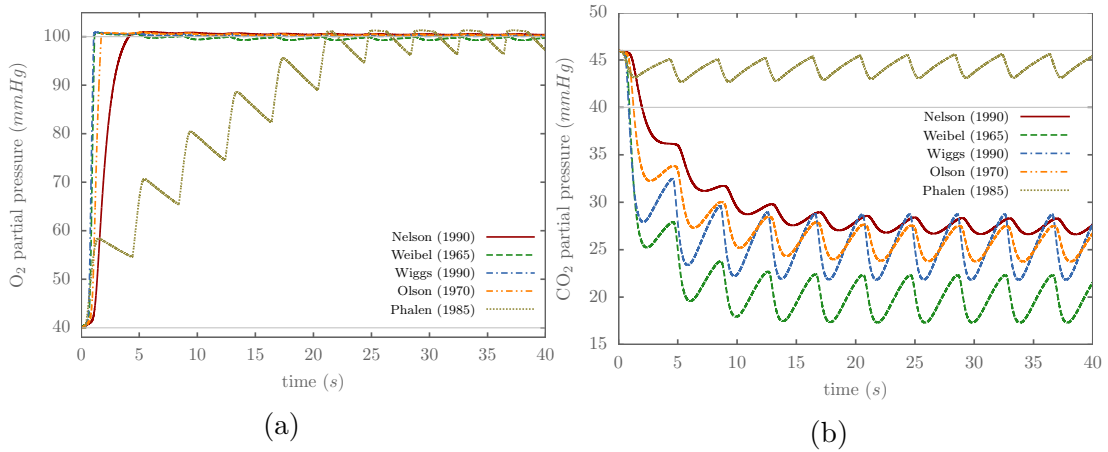


Figure 4.2: Comparison of the time variation of the mean partial pressure of Oxygen (left) and carbon dioxide (right) in the blood capillary of adults for the different airways geometry models.

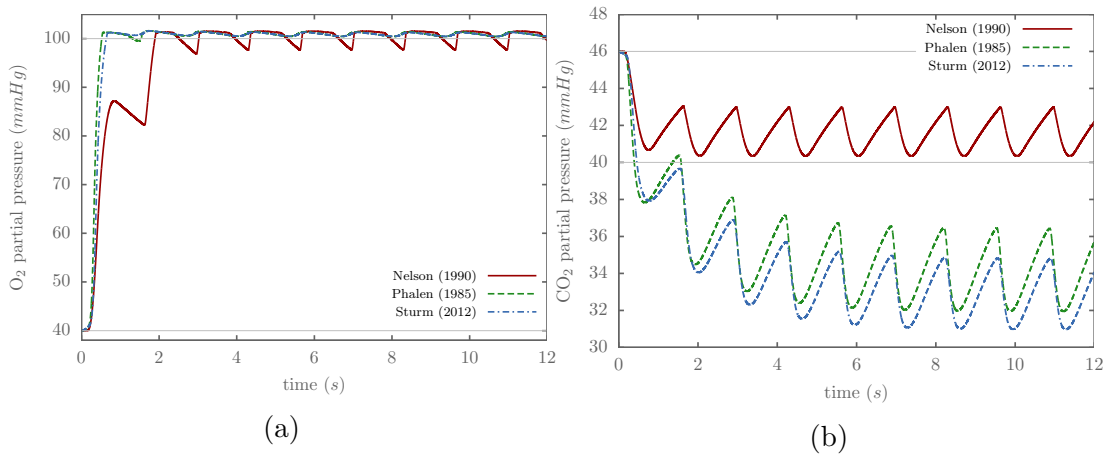


Figure 4.3: Comparison of the time variation of the mean partial pressure of Oxygen (left) and carbon dioxide (right) in the blood capillary of infants for the different airways geometry models.

Impact of the lung resistance and compliance on gas exchange with the blood is captured through the time constant of the mechanical model, $\tau = \mathcal{R}\mathcal{C}$. This time scale, listed in table 4.3 for the various airways geometries, characterizes how fast the system responds to changes in the driving pressure difference in term of the air volume exchange. The compliance, a property of the lung tissue, is taken to be the same for all adults (infants) scenarios since these only differ in terms of airways geometry. Dominated by the airways, the resistance is, however, directly dependent on the airways geometry. This implies that it suffices to use the resistance to compare the speed of volume exchange for the various adults

(or infants) cases.

Table 4.2 shows that the resistance estimated for the various airways geometries for adults are well below the range of reported measurements (1.08-2.6 $cmH_2O.s/L$), except for [2], where the resistance (1.49 $cmH_2O.s/L$) is within the range. Figures 4.2a also show that for airways of smaller resistance, the mean partial pressures of oxygen and carbon dioxide are faster to reach the quasi-stationary state. The only exception is for the case of [12], where although the estimated resistance (0.357 $cmH_2O.s/L$) is well below the range of reported measurements (1.08-2.6 $cmH_2O.s/L$), it takes more than 20 seconds for oxygen partial pressure in the blood to reach the quasi-stationary behavior. The partial pressure of carbon dioxide, however, reaches its quasi-stationary behavior quickly because its value at the initial condition is very close to its value at the quasi-stationary state. As for the infants, the estimated resistance of [2] is well above the range (22.6-52 $cmH_2O.s/L$), while those of [12] and [15] are well below. As a consequence, it takes less than 1 second for the blood to be saturated with oxygen for the airways geometries of [12] and [15], while it takes more than 2 seconds for the geometry of [12]. A key characteristic of all the airways geometries (except [12]) with resistances well below the range of reported measurements is that the partial pressure of carbon dioxide in the blood oscillates, at quasi-steady state, over a range well below the nominal range (40-46 $mmHg$). Discussion of the peculiar behavior of the adult airways geometry reported in [12] that resulted in poor removal of carbon dioxide from the blood is presented below. Abnormally elevated carbon dioxide levels in the blood are typically caused by hypoventilation, whereas reduced levels are typically caused by hyperventilation. Based on this, we can categorize the airways geometries in table 4.2 as either hyperventilating or hypoventilating.

Note that we excluded [13] and [11] from the results in figure 4.2 due to their very high dead space volumes and very small resistance, as can be seen in table 4.2.

One can also observe from table 4.2 that a higher dead space volume does not always lead to a smaller airways resistance, and vice versa, as can be seen by comparing cases I and J (or A and B) of table 4.2. For a given circular channel of length L and diameter D , both the channel volume and the resistance would increase if L is increased a factor $\alpha > 1$ and D is increased by a factor β that satisfies $\alpha^{-1/2} < \beta < \alpha^{1/4}$.

Since the length and diameter of the airways channels decrease for higher generations, the air flow and species transport become increasingly dominated by diffusion, approaching the Stokes flow regime in the last generation, as indicated by the low values of Reynolds and Peclet numbers listed in table 4.3. This implies

that the diffusion term $\mathcal{D}_{\bullet,air} A_{in} \left. \frac{\partial C(x,t)}{\partial x} \right|_{in}$ in equation (3.9) plays a significant role in transporting Oxygen and Carbon Dioxide into and out of the alveolar space. This diffusion term depends on two main parameters which are related directly to the geometry of the models: (i) the concentration gradient $\left. \frac{\partial C(x,t)}{\partial x} \right|_{in}$ which is affected by the distribution of the species along the airways and (ii) the airways inlet area to the alveolus $A_{in} = \frac{2^{N_g-1} \pi D_{N_g}^2}{4N_a}$, where N_g is the number of generations, D_{N_g} is the diameter of the last generation, and N_a is the number of alveoli. Among the cases presented in figure 4.2b, we notice that the airways geometry that results in the lowest carbon dioxide levels in the blood is [10] has the highest A_{in} (or R_{in}/R_{alv} , $A_{in} = \pi R_{in}^2$), as shown in Table 4.3. We also notice that the airways geometry of [12] yielded the highest carbon dioxide levels in the blood, where A_{in} (or R_{in}/R_{alv}) is lowest. The difference in CO2 removal from the blood between the airways geometries of [10] and [12] is attributed to the fact the first consists of 24 generations, while the second consists of 16 generations only, while both share nearly similar values of the terminal branch diameter. The impact of the small alveolar inlet of [12] can also be seen in Figure 4.2a, where the small flux at the alveolar inlet causes the oxygenation to be very slow, where it takes 22 seconds (6 respiration cycles) for the blood to reach saturation.

In figure 4.2b, we notice that the mean partial pressure of carbon dioxide in the blood using the airways geometry model of [2] undergoes small fluctuation amplitude around a mean that is higher than that of all other 24-generation models. This is attributed to the overestimated lengths of the generation (14-25), as can be seen in Figure 2.1 (or Table 2.1). Increasing the lengths (L_i) of the generations where diffusion is dominant results in a smaller species flux at the alveolar inlet, since $\frac{\partial C(x,t)}{\partial x} \sim \frac{1}{\sum L_i}$. This damping effect results in smaller fluctuation amplitudes and overall reduction in gases exchange.

Figures 4.4 and 4.5 show the partial pressure of oxygen and carbon dioxide along the capillary every one eighth of a respiration period at the quasi-stationary state using the airways models of [1] for adults and [2] for infants. The fluctuations in time of the mean, averaged along the capillary, has already been discussed using Figures 4.2 and 4.3. It can be seen the in both cases, the concentrations reach their fully developed state maximum values over a distance that is less than one fifth of the capillary length.

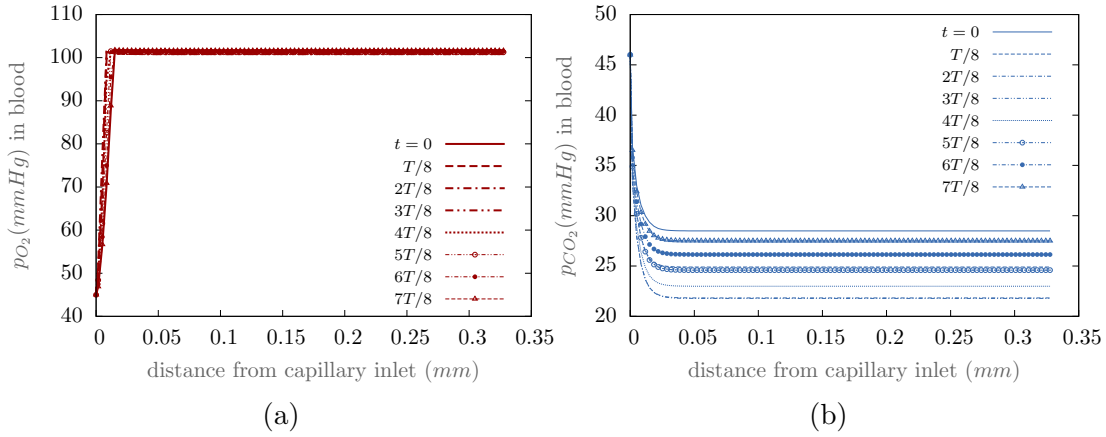


Figure 4.4: Variation of the oxygen and carbon dioxide partial pressured in the blood along the capillary over one complete cycle (period T) for adults using the airways geometry in [1].

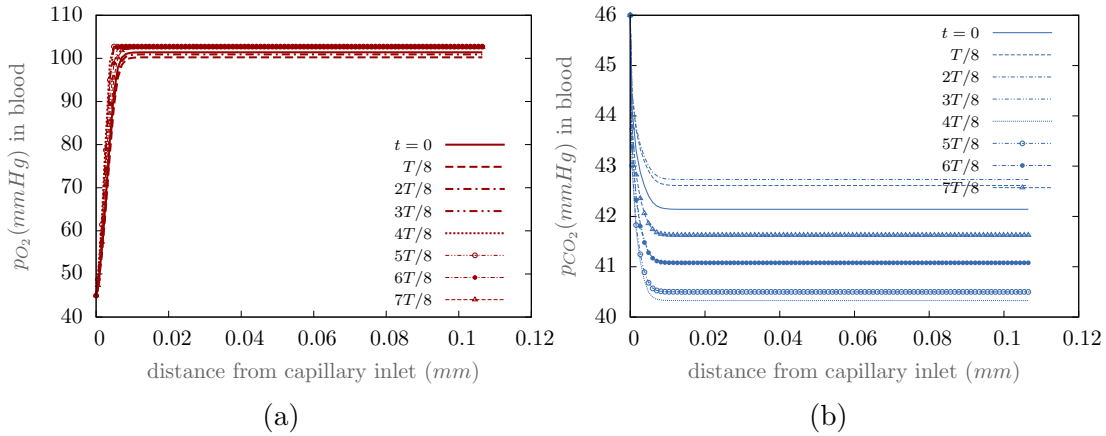


Figure 4.5: Variation of the oxygen and carbon dioxide partial pressured in the blood along the capillary over one complete cycle (period T) for infants using the airways geometry in [2].

4.1 Discussion

Quantitative description of the tracheobronchial airway morphometry is essential for the investigation of toxicologic effects of inhaled aerosols and gases under a variety of conditions. Limitations in measurements prohibit the accurate estimation of the dimensions of the generations beyond the first few. As a result, some studies opted to include only the first few generations in their design, while others relied on inferred dimensions for the rest of the generations, as discussed in the Introduction and Materials and Methods sections. Inaccurate measurements

and corresponding quantitative descriptions of the airway anatomy undermine the ability of the associated dosimetry models in animal toxicology to accurately predict particle transport and deposition dynamics within the respiratory tract.

Accurate predictions of the exchange of inhaled aerosols and gases with the blood in the pulmonary capillaries are not possible without a physically sound representation of the airways dimensions. Such predictions require both an adequate pulmonary tree representation and a model to predict the dynamics of air and gases transport all the way to the alveoli. A properly constructed mathematical representation of these processes not only enhances our understanding of pulmonary diseases, but it also enables investigation of many what-if scenarios.

We postulate that a physically sound representation of the airways dimensions should meet geometrical, mechanical, and species transport requirements. Any geometric representation of the tracheobronchial airway morphometry should conform to high-fidelity observable geometric quantities such as the dimensions of the first few generations, dead space volume, and path length. Such a representation should also reproduce high-fidelity observables that characterize the mechanical behavior such as resistance and inductance. The associated lung mechanics model must also reproduce high-fidelity observables, including the tidal volume under normal breathing conditions. A key contribution of this study is its assessment of the airways geometric models in terms of gas transport along the respiratory tract and the eventual exchange with blood in the capillaries across the alveolar membrane. Specifically, a proper representation of the airways dimensions must ensure that the predicted dynamics of oxygenation and carbon dioxide removal in the blood agrees with observations. We found out that overestimating the lengths of the generations where diffusion is dominant results in a smaller mass fluxes at the alveolar inlet. This damping effect results in smaller fluctuation amplitudes and in overall reduction in gas exchange. We also found out that the area of the airways inlet to alveolus (terminal bronchiole diameter) plays a key role in the gases exchange. Thus extra care must be taken when reporting these dimensions.

A suitable computational and/or experimental model that employs a physically sound representation of the airways dimensions can be ultimately used to design patient customized ventilation modalities, where the model is periodically updated with in vivo observations. We should not, however, ignore the fact the computational and/or experimental methods that incorporate the airways geometry used should be sufficiently accurate in a way that is compatible with the objectives and scope of a particular study.

Appendix A

Model Parameters

The respiratory system consists of the airways and the lung. The airways are divided into two components: the extrathoractic and the intrathoractic airways. The extrathoractic (superior) airway includes the supraglottic, glottic and infraglottic regions. The intrathoractic (inferior) airway includes the trachea, the main bronchi, and the rest of the bronchial generations, which have as their main function the conduction of air to the alveolar surface[48] .

Table A.1 list the parameters used by the various submodels. Note that the value of each parameter can be directly specified or estimated using the relations and data collected from the literature.

Table A.1: Model parameters.

parameter	submodel	estimation
Initial alveolus thickness	alveoli geometry	$0.6 \mu m$
Capillary diameter	blood circulation	$10 \mu m$
Capillary to alveolus contact area ratio	alveolar membrane transport	0.3
Transit time of blood in capillary	capillaries transport	$1 sec$
Capillary length to half alveolus perimeter ratio	alveolar membrane transport	1
Inspiration to expiration ratio	mechanical model	0.5
Maximum intrapleural pressure	mechanical model	$-5 cmH_2O$
Minimum intrapleural pressure	mechanical model	$-10 cmH_2O$
O_2 concentration at airways inlet	airways transport	$0.3762 kg/m^3$
CO_2 concentration at airways inlet	airways transport	$0.0067 kg/m^3$
O_2 partial pressure at capillary inlet	capillaries transport	40 mmHg
CO_2 partial pressure at capillary inlet	capillaries transport	46 mmHg

A.1 Nominal mass and height

Many model parameters are expressed in terms of mass and height. Unless otherwise specified, the mass (kg) and height (cm) are determined as a function of age and sex. This is done by incorporating into the model the growth charts [49] for both males and females from the age of few days till the age of 20. Based on the USA population, the growth charts provide the mass and height at various percentiles given the age and sex. The nominal mass and height, taken to be at the 50th percentile, are plotted again age in Figures A.1 and A.2 respectively and in Figures A.3 and A.4 for infants up to an age of 40 months.

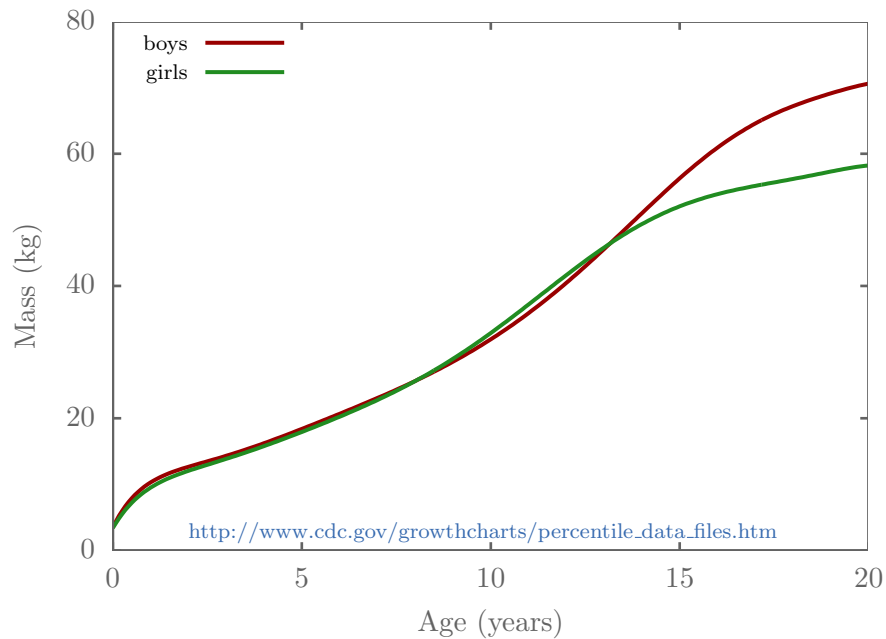


Figure A.1: Nominal mass versus age.

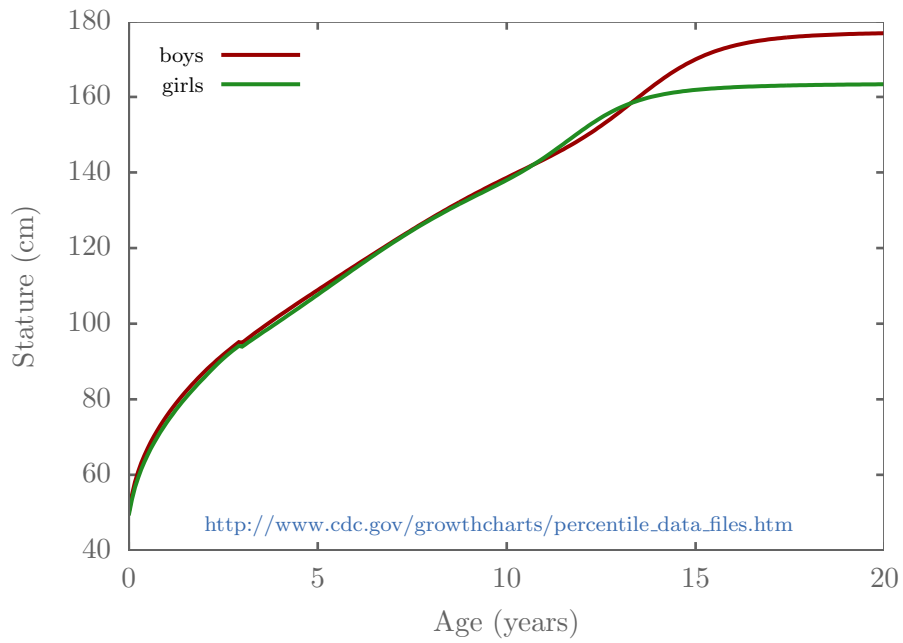


Figure A.2: Nominal height versus age.

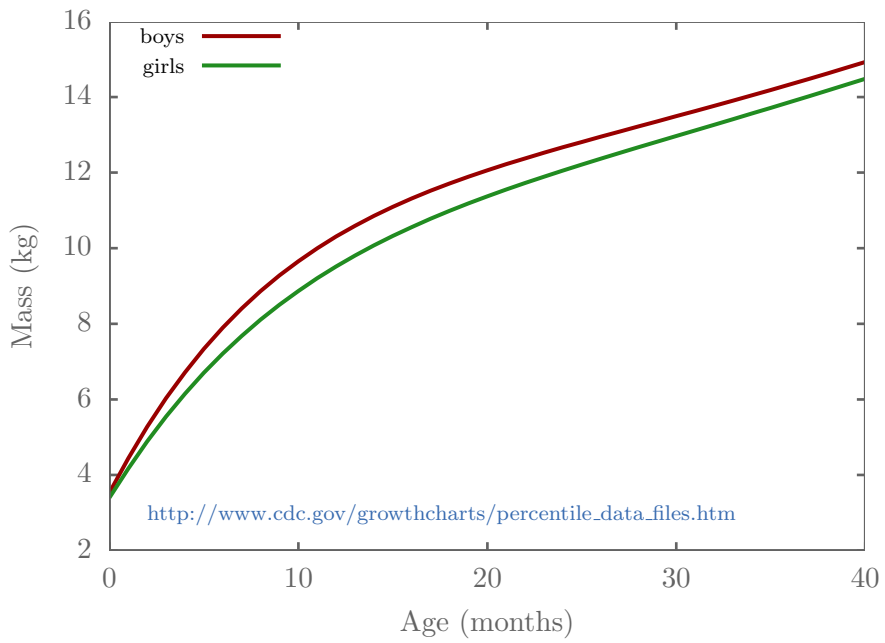


Figure A.3: Nominal infant mass versus age.

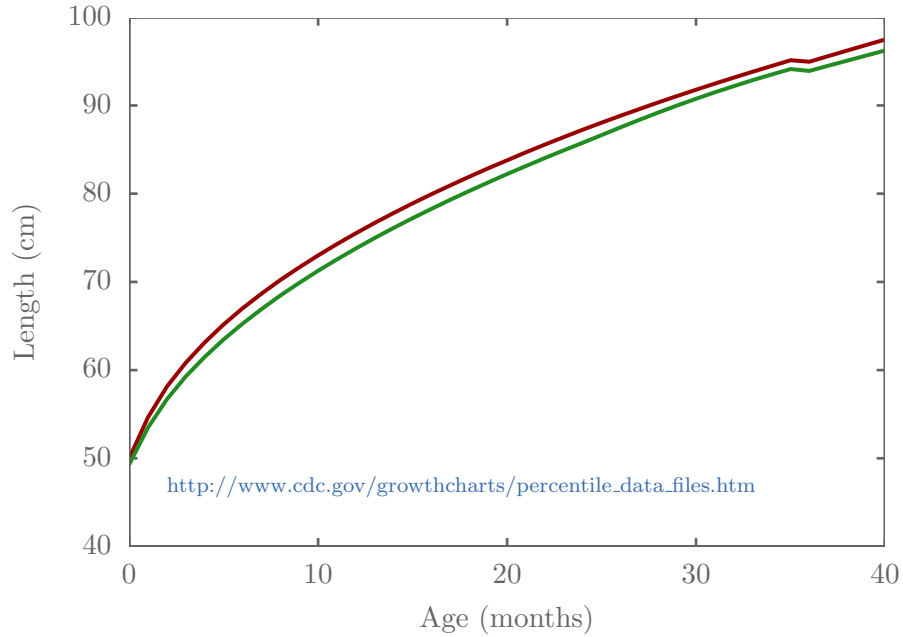


Figure A.4: Nominal infant height versus age.

A.2 Respiration Frequency

Ventilation rates and volumes may be thought of as responses of the lung mechanical model to the difference between the inlet pressure and the intrapleural pressure. Under normal conditions, the inlet pressure is atmospheric and breathing is driven by a periodic change in the intrapleural pressure. The intrapleural pressure signal is characterized by its frequency, the respiration frequency, and the peak-to-peak difference, $p_{ip,max} - p_{ip,min}$. The respiration frequency is thus a significant parameter as it impacts the tidal volume and the rates at which oxygen and carbon dioxides are exchanged between the alveolar space and the environment. Dependence of the frequency of respiration on age, as reported in different sources, is plotted in Figure A.5. An infant naturally breathes at frequencies higher than an adult. Higher respiration rates are typically accompanied with smaller volume intakes.

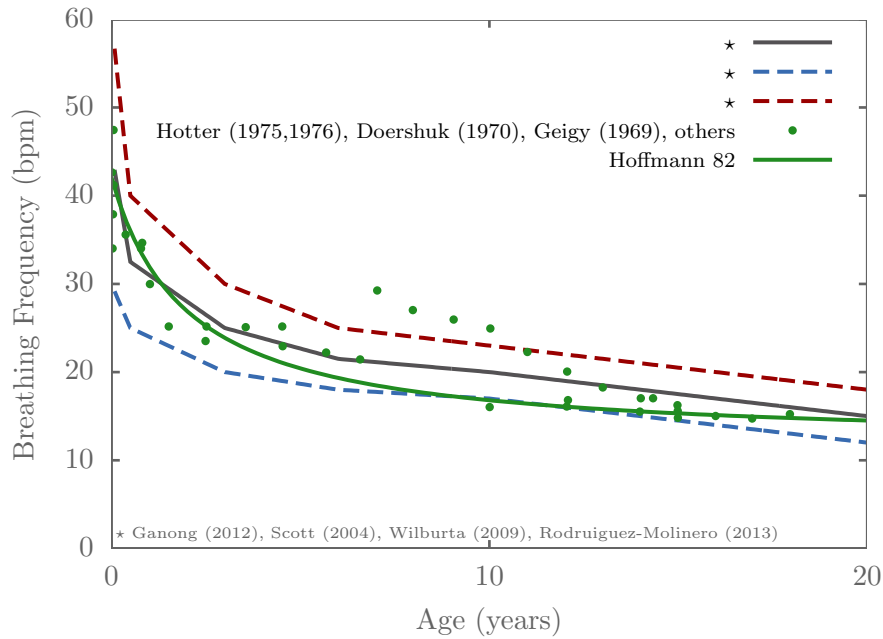


Figure A.5: Frequency of respiration versus age.

A.3 Trachea and main bronchi: length and diameter

The first two generations of the airways are the trachea and the main bronchi. In many cases, the trachea diameter and length are measured separately from the rest of the airways. Figures A.6 and A.7 show respectively the dependence on age of the diameter and length of the trachea and main bronchi, as reported in difference references. The trachea length is often estimated as 5 times the diameter, based on Yeh et Schum (1980) [50].

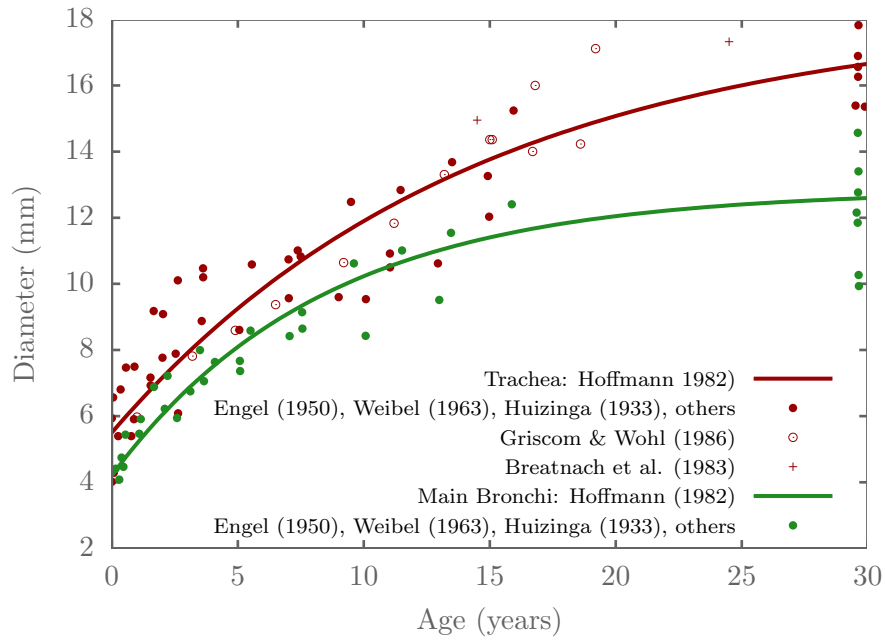


Figure A.6: Trachea diameter versus age. [3] reported length and diameter of trachea vs age for 130 children and adolescents. [4]: 808 patients (430 males and 378 females).

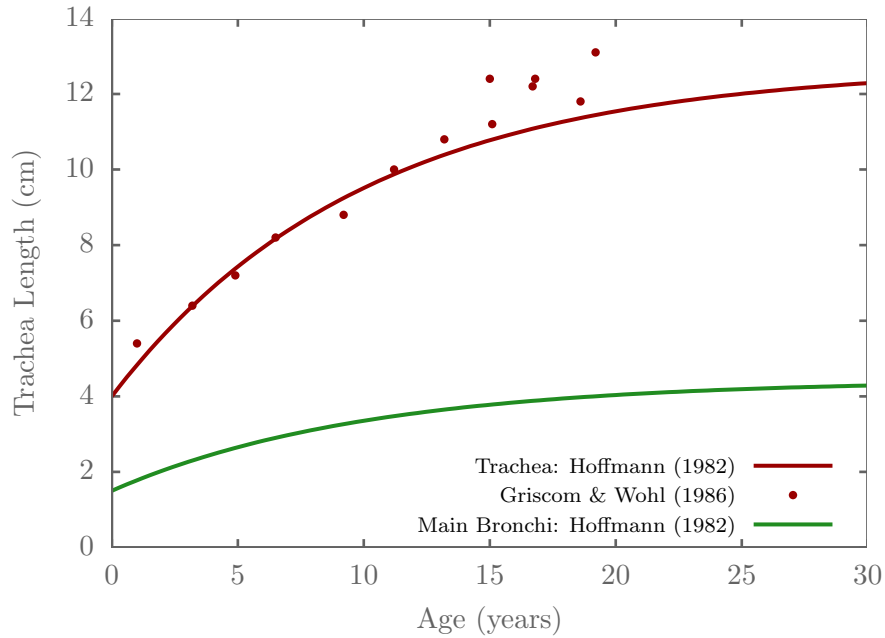


Figure A.7: Trachea length versus age. [5]: $\text{length}(\text{cm}) = 0.0856 * \text{height}(\text{cm}) - 2.32$. [3] reported length and diameter of trachea vs age for 130 children and adolescents.

A.4 The Number of Alveoli

The alveoli are open chambers in a complex 3D maze formed by the alveolar walls [51]. Each alveolus has one opening towards an alveolar duct, framed by an entrance ring formed of the strong fiber tracts in the free edges of the alveolar septa. In our model, the average volume of a single alveolus is determined by dividing the total alveolar volume by the number of alveoli. At the end of expiration, the total alveolar volume is the difference between the functional residual capacity (FRC) and the dead space (DS). Correlations for the FRC and DS, in addition to other lung volumes, are presented below in A.5. One of the earlier model-based counting methods can be found in [52]. The method, which requires assumptions of shape and size distribution factors, resulted in an estimate of 300 million alveoli in the average human lung. A more accurate estimate of 480 million alveoli is reported in [37], which used stereological analysis[53, 54] for counting. [37] reports that [38] and [6] seems to have more accurate estimates than older measurements. Another recent study done by [55] reports the number of alveoli using advanced stereological counting technique. According to [6], the number of alveoli follows a logarithmic growth with age and depends on gender, with males having slightly more alveoli than females at a certain age. The number of alveoli, in millions, is correlated as follows:

$$\begin{array}{ll} \text{males} & NALV = 311.2 + 62.79 \ln(A) \\ \text{females} & NALV = 269.4 + 55.49 \ln(A) \end{array} \quad (\text{A.1})$$

This correlation suggests that the number of alveoli increases significantly from around 30 million for a preterm infant to 500 million in a 20 years old adult. Further change in the number of alveoli for ages larger than 20 years is insignificant. Table A.2 lists various sources that reported measurements of the number of alveoli ($NALV$) and its dependence on age and/or lung volume.

Table A.2: Data collected on number of alveoli in healthy subjects from different sources. gwk stands for gestation weeks. pnwk: postnatal weeks.

source	measurement	no. of subjects	age range	gender
[56]	$NALV(Age)$	3	0-8 yr	
[56]	$NALV(Age, LV)$	5	0-11 yr	
[57]	$NALV(LV)$	32	19-85 yr	
[58]	$NALV(Age)$	14	< 19 yr	
		32	adults	
[6]	$NALV(Age)$	20	6 wk - 14 yr	girls
		36	6 wk - 14 yr	boys
[38]	$NALV(Age, LV)$	5	29 gwk -18 pnwk	
[37]	$NALV(LV)$	6	adults	
[55]	$NALV(Age)$	11	0.09-15.9 yr	

Figure A.8 shows the dependence on the number of alveoli on age, using data and models collected from the studies listed in Table A.2. Dependence over an age range of 20 gestation weeks to 50 postnatal weeks is shown in Figure A.9. A log-log plot, that highlights the logarithmic growth in the number of alveoli per unit lung volume with age, is shown in Figure A.10.

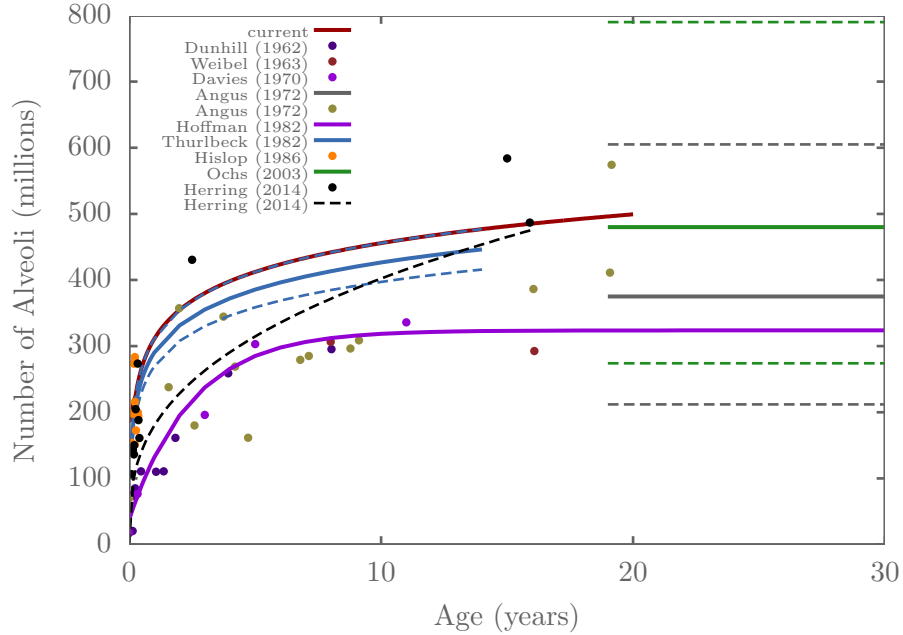


Figure A.8: Number of alveoli vs age from various references.

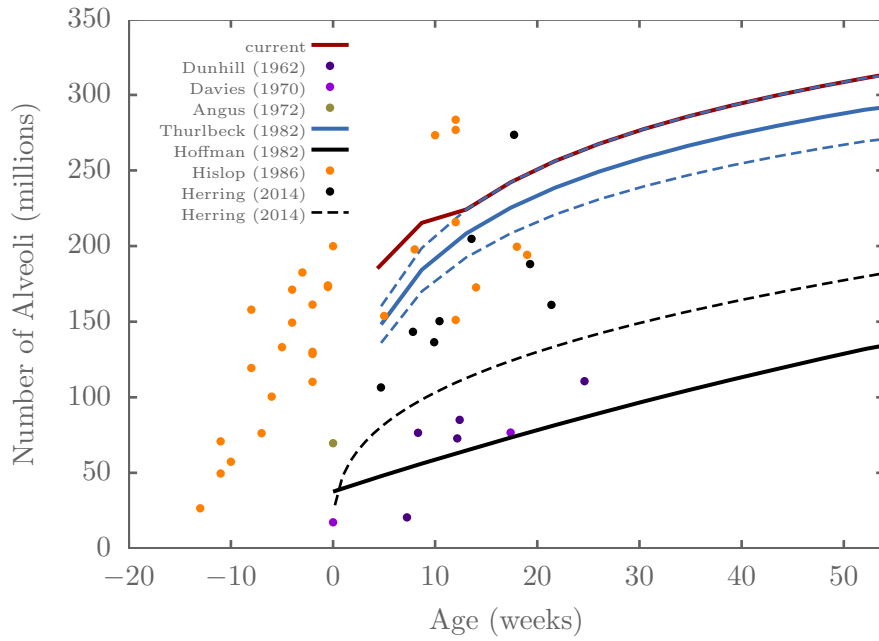


Figure A.9: Number of alveoli vs age from various references.

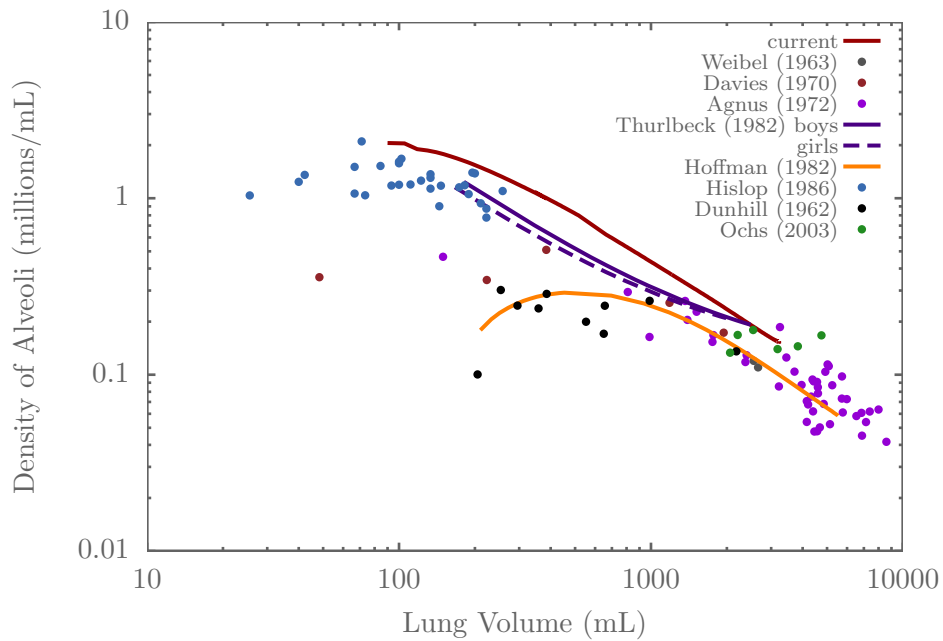


Figure A.10: Number of alveoli per unit lung volume vs total lung volume from various references.

A.5 Lung Volumes

Nominal values for the lung volumes are needed to get many important parameters such as the nominal lung tissue compliance, nominal airways resistance, and the volume of the lung at the open pressure (which is normally the maximum intrapleural pressure of $-5 \text{ cmH}_2\text{O}$). The lung volumes that are used by our model are the tidal volume, functional residual capacity, and the dead space.

Various lung volumes are usually measured experimentally for individuals of different ages, weights, heights, and sex [59, 60, 61]. Note that in the following equations, A is the age in years, BW is the weight in Kg, H_{cm} is the height in cm, and H is the height in m. Correlations for these volume in terms of these parameters, in addition to sex, are presented next.

A.5.1 Tidal volume

The nominal tidal volume (TV_{nom}) is the tidal volume under normal breathing conditions of a healthy person. Correlation for the tidal volume as a function of age can be found in [62]. This correlation, along with data from other sources, is plotted in Figure A.11. The nominal tidal volume is usually measured per unit body weight and is estimated to be 4-5 mL/Kg in newborn babies, increasing to about 7 mL/Kg in adults[63]. For a 71 kg adult, the tidal volume is around 500 mL, in agreement with [64]. For a 3 kg infant, the tidal volume is about 15 mL[65]. [8] reported the tidal volume vs Height as $TV(ml) = 4.19H(cm) - 206.6$. To produce the plots in the figure, the growth charts [49] (50th percentile) were used to relate age to mass and height.

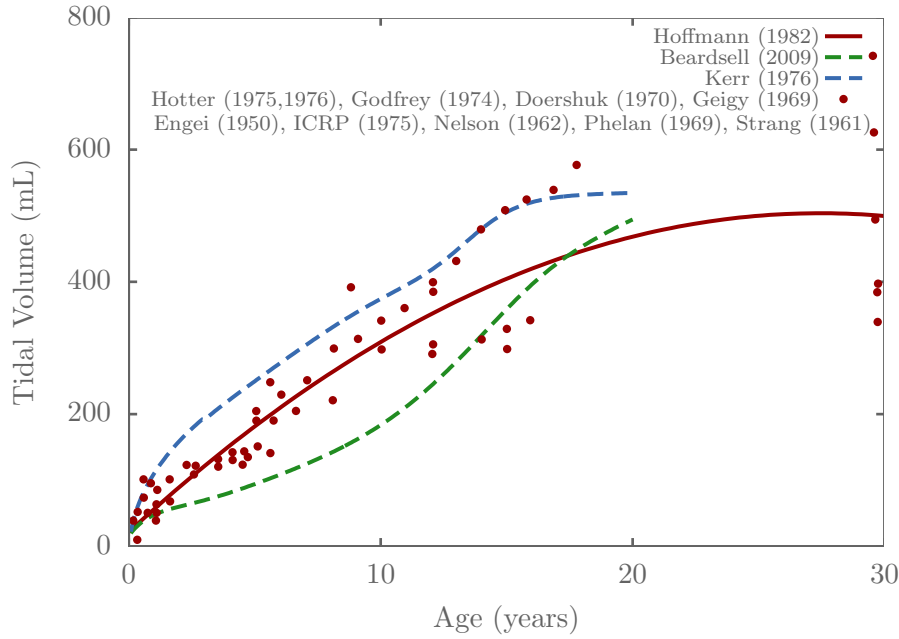


Figure A.11: Nominal tidal volume versus age.

The nominal tidal volume may be used to calculate the nominal compliance as

$$C_{nom} = \frac{TV_{nom}}{p_{ip,max} - p_{ip,min}} \quad (\text{A.2})$$

where $p_{ip,max} - p_{ip,min}$ are respectively the maximum and minimum intrapleural pressure during a breathing cycle under normal conditions.

A.5.2 Functional Residual Capacity

The Functional Residual Capacity (FRC) is particularly important since it allows estimation of the the alveolar volume (AV) as

$$AV = FRC - DS \quad (\text{A.3})$$

where DS is the dead space, discussed in section A.5.3. The alveolar volume is, in turn, used to estimate the volume of a single alveolus at the end of expiration as $AV/NALV$, where $NALV$ is the number of alveoli. Table A.3 and Figure A.12 shows dependence of FRC on height using data from various sources.

Table A.3: Data collected on FRC for both genders from different sources. M: male, F: female, P: plethysmography, MS: Mass spectrometry, U: Ultra sonic, H: Helium dilution, W: Washout.

Source	Age range (Method)	no. of subjects	gender	Equation/ mean
[66]	6-14 yr	93		$0.92 \times 10^{-6} H_{cm}^{2.86}$ L
[67]	5-38 yr	171	M	$0.125 \times 10^{-3} H_{cm}^{3.298}$ mL
			F	$0.286 \times 10^{-3} H_{cm}^{3.136}$ mL
[68]	7-15 yr	45		$2.11 \times 10^{-7} H_{cm}^{3.103}$ L
Doershuk & Matthews (1969)	0-0.1 mo	49		89.5 ± 15.5 mL
[69]	1-23 mo	25		$1.57 \times 10^{-5} H_{cm}^{2.23}$ L
[70]	4-16 mo	35		$5.5 H_{cm} - 141.6$ mL
[71]	0.1-12 mo	48		$6.78 H_{cm} - 2.28 \times 100$ mL
[72]	2-7 yr	63		$13.85 H_{cm} - 886$ mL
[73]	18-86 yr	179	M	$7.502 H_m - 7.608$ L
			F	$5.867 H_m - 5.972$ L
[74]	0.1-31 mo	110		$e^{-5.91} H_{cm}^{2.59}$ mL
[75]	0.74-60 wk	69		$5.16 H_{cm} - 175.72$ mL
[60]	0-8 yr	569		$1.4 \times 0.0031 H_{cm}^{2.56}$ mL
[76]	1-26 mo (P)	27		$e^{-6.21} H_{cm}^{2.69}$ mL
	1-26 mo (H)	27		$e^{-6.53} H_{cm}^{2.74}$ mL
[77]	23-46 yr (P)	9		3.3 ± 0.8 L
	23-46 yr (W)	9		3 ± 0.85 L
[78]	20-70 yr	482	M	3420 ± 765 mL
			F	2841 ± 555 mL
[79]	20-80 yr	100	M	$2.78 H_m - 1.83$ L
			F	$1.3 H_m + 0.21$ L
[80]	18-88 yr	591	M	3.18 ± 0.76 L
			F	2.36 ± 0.52 L
[81]	3-120 wk	22		$303.7 - 8.89 H_{cm} + 0.105 H_{cm}^2$ mL
[82]	38.3 ± 9.2 d	12		79.2 ± 1.2 mL
[83]	4-93 wk	32		$0.02 H_{cm}^{2.1572}$ mL

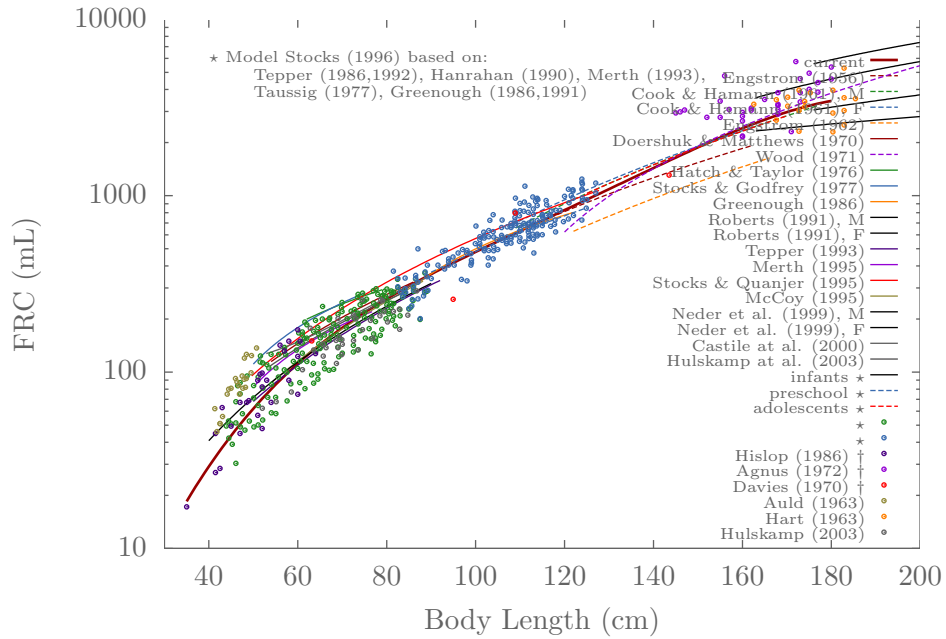


Figure A.12: Functional residual capacity versus body height (measurements and relations). Converting from total lung volume to FRC is done by using the correlation by [6] of FRC dependence on lung volume and age, as plotted in Figure A.13.

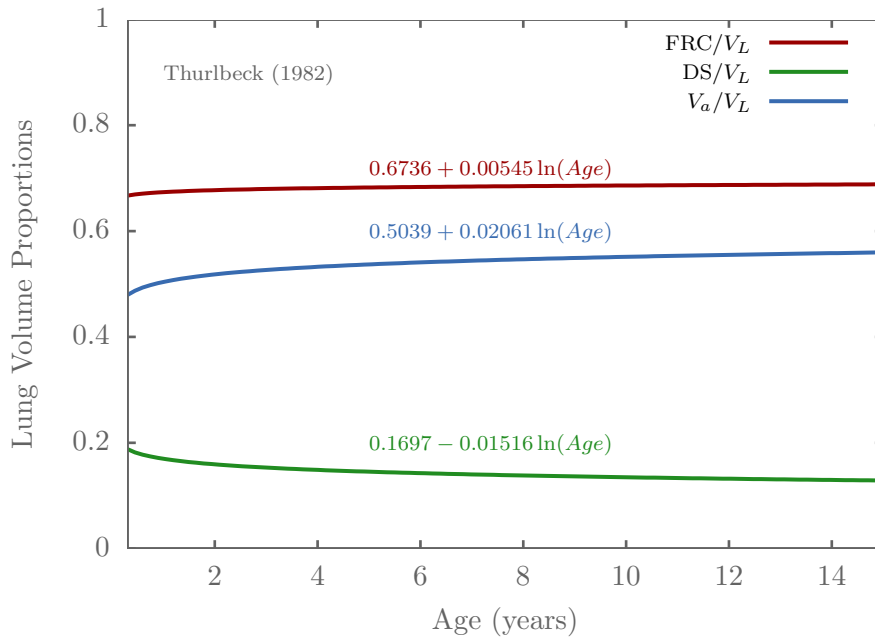


Figure A.13: Lung volume fractions as a function of age [6].

A.5.3 Dead Space

Dead space corresponds to the air space in regions of the lung where no gas exchange occurs. The (total) physiologic dead space (DS) is the sum of the anatomic dead space ($DSAN$) and the alveolar dead space ($DSAV$). The alveolar dead space is sum of the volumes of those alveoli which are not involved in gas exchange with the blood. According to [46] it is accepted in adults that ($DSAN$) and (DS) are virtually identical in normal lungs. A similar relationship that holds for children has been assumed by [84]. The anatomic dead space, consisting of intrathoracic (DSI) and extrathoracic (DSE) (outside the chest) components[7], is that portion of the airways which conducts gas to the alveoli. [7] argues that, because infants and children head is large, the proportion of the extrathoracic dead space is larger. Table A.4 lists correlations for extrathoracic and total dead spaces as a function of mass and age, obtained from various sources.

Table A.4: Correlations for DS , DSE and DSP . Note that the $DSI = DS - DSE$. DSP : Physiological dead space. A: Asthmatic, CF: Cystic fibrosis, I: Intubated with cuffed endotracheal tubes, V: Ventilated.

source	Age Range (Health)	no. of subjects	quantity	expression/ value
[9]	4 - 42 yr	73	$DSAN$	$7.585 \times 10^{-4} H_{cm}^{2.363} \text{ mL}$
[8]	5-16 yr	72	$DSAN$	$1.018 H_{cm} - 76.2 \text{ mL}$
	5-16 yr	52	DSP	$1.707 H_{cm} - 72.5 \text{ mL}$
	children (A)	42	$DSAN$ and DSP	
	children (CF)	28	$DSAN$ and DSP	
[7]	7 d - 14.2 yr (I)	40	$DSAN$	$3.28 - 0.56 \ln(1 + Age(yr)) \text{ mL/kg}$
	7 d - 14.2 yr (I)	40	DSE	$1.64 - 0.242 \ln(Age(yr)) \text{ mL/kg}$
	18 d- 14.7 yr (V)	10	DSI	1.03 mL/kg
[85]	7-40 yr	19	$DSAN$	$4.5 \times 10^{-5} H_{cm}^{2.92} \text{ mL}$
	children (A)	22	$DSAN$	
	children (CF)	11	$DSAN$	
[86]	adults		$DSAN$	
[87]	adults		$DSAN$	

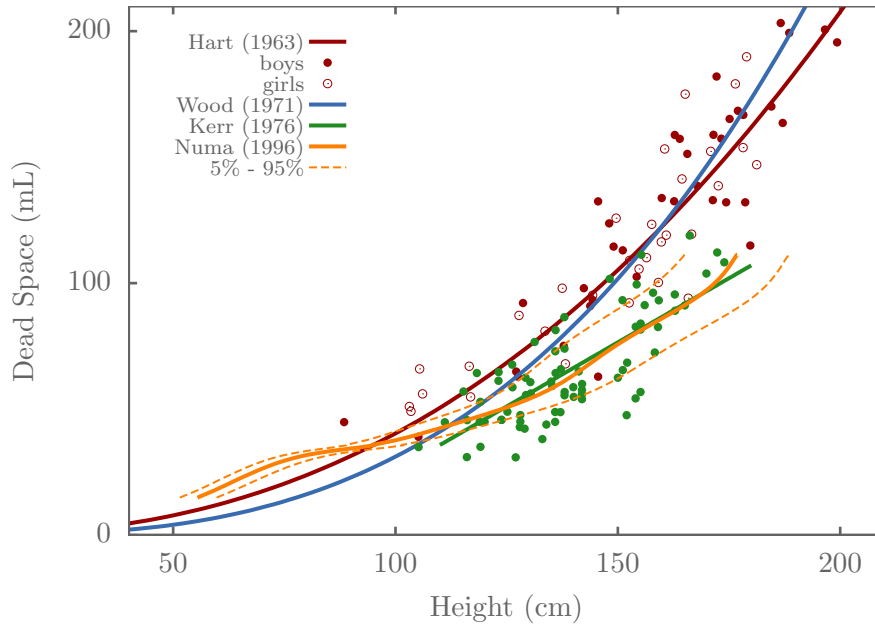


Figure A.14: Dead space volume versus body length from [7],[8],[9]. When needed, growth charts were used to express height as a function of age.

Measurements of the dead space volume for adults and infants, reported from various sources, are presented in Tables A.5 and A.6.

Table A.5: Measurements of the dead space volume for adults (m : men, w : women).

Reference	DS ($cmH_2O \cdot s^2/l$)
[88]	156 ± 28^m 104^w
[89]	150-200
[90]	180.8 ± 32^m 126.9 ± 26.7^w
[91]	167 ± 38^m 138 ± 24^w
[92]	190 ± 30 170 ± 40
[93]	197.7 ± 33.2^V

Table A.6: Measurements of the dead space volume for infants. *calculated from age dependent correlations. P: Preterm birth. V: Ventilated.

Reference	\mathcal{DS} ($cmH_2O.s^2/l$)
[8]	27*
[94]	6.4 ± 1.33^V
[95]	3.08 ± 1.06^P
[96]	6.7
[97]	6.1 ± 0.4
	5.18 ± 0.12^P
[7]	11.57*
[98]	4.15 ± 2^V
[99]	5.1
	4.6^P

A.6 Lung Mechanical Model Parameters

These are the compliance and resistance.

A.6.1 Compliance

The compliance of the tissue is a measure of how much the lungs inflate with a given pressure difference in the chest cavity. In the mechanical model, the compliance is either measured or computed from a compliance model that accounts for the viscoelastic behavior of lung tissues including surface tension in the alveoli. During a normal inspiration, the human being intakes the nominal tidal volume, driven by a drop (typically $5\text{ cmH}_2\text{O}$) in the intrapleural pressure. The nominal compliance may then be inferred from the tidal volume and the peak-to-peak change in intrapleural pressure as

$$\mathcal{C}_{nominal} = \frac{TV}{p_{ip,max} - p_{ip,min}} \quad (\text{A.4})$$

Equation (A.4) can be derived from Equation (3.1) by observing that at the beginning and end of inspiration, dV/dt is very small.

A.6.2 Resistance

In the mechanical model, the resistance is either measured or computed from a resistance model, which, in turn, takes the airways geometry and flow conditions as input. If we assumed fully developed laminar flow conditions in all the airways channels, the nominal resistance may then be expressed as

$$\mathcal{R}_{nominal} = \sum_{k=0}^{N_g} \frac{128\mu L_k}{\pi D_k^4 2^k} \quad (\text{A.5})$$

Measurements of the total resistance for adults and infants, reported from various sources, are presented in Tables A.7 and A.8.

Table A.7: Measurements of total resistance, dead space volume, and inductance for adults (m : men, w : women).

Reference	\mathcal{R} ($cmH_2O.s/l$)
[100]	1.5 ± 0.49
[101]	1.53 ± 0.64
[102]	1.35 ± 0.53
[103]	1.08
[104]	1.67 ± 0.61
[105]	1.8^m 2.22^w
[106]	2.32 ± 0.6^m 2.6 ± 0.6^w

Table A.8: Measurements of total resistance, dead space volume, and inductance for infants. **Inspiration-Expiration. P: Preterm birth.

Reference	\mathcal{R} ($cmH_2O.s/l$)
[107]	29 ± 12.9
[108]	26 ± 6.5
[109]	18.1 ± 6.3
[110]	38.5 ± 25.2
[111]	47.5 ± 5.6
[112]	25 ± 7.7 - $36 \pm 7.8^{P**}$
[113]	25.4 ± 3.3
[114]	52-70**
[115]	22.6 ± 8.9
[116]	35.62 ± 1.94
[117]	28.68 ± 8
	34.84 ± 13.01
[95]	48.8 ± 15.4^P
[118]	54.8 ± 15

Bibliography

- [1] B. R. Wiggs, R. Moreno, J. C. Hogg, C. Hilliam, and P. D. Pare, “A model of the mechanics of airway narrowing,” *J. Appl. Physiol.*, vol. 69, no. 3, pp. 849–860, 1990.
- [2] T. R. Nelson, B. J. West, and A. L. Goldberger, “The fractal lung: universal and species-related scaling patterns,” *Experientia*, vol. 46, no. 3, pp. 251–254, 1990.
- [3] N. Griscom and M. Wohl, “Dimensions of the growing trachea related to age and gender,” *American Journal of Roentgenology*, vol. 146, no. 2, pp. 233–237, 1986.
- [4] E. Breatnach, G. C. Abbott, and R. G. Fraser, “Dimensions of the normal human trachea,” *American Journal of Roentgenology*, vol. 142, no. 5, pp. 903–906, 1984.
- [5] N. T. Griscom and M. E. B. Wohl, “Dimensions of the growing trachea related to body height: Length, anteroposterior and transverse diameters, cross-sectional area, and volume in subjects younger than 20 years of age 1–3,” *American Review of Respiratory Disease*, vol. 131, no. 6, pp. 840–844, 1985.
- [6] W. M. Thurlbeck, “Postnatal human lung growth,” *Thorax*, vol. 37, pp. 564–571, 1982.
- [7] A. H. Numa and C. J. Newth, “Anatomic dead space in infants and children,” *J. Appl. Physiol.*, vol. 80, no. 5, pp. 1485–1489, 1996.
- [8] A. A. Kerr, “Dead space ventilation in normal children and children with obstructive airways disease,” *Thorax*, vol. 31, no. 1, pp. 63–69, 1976.
- [9] M. Hart, M. Orzalesi, and C. Cook, “Relation between anatomic respiratory dead space and body size and lung volume,” *Applied Physiology*, vol. 18, pp. 519–522, 1963.
- [10] E. R. Weibel, *Morphometry of the human lung*. Springer, 1965.

- [11] K. Horsfield and G. Cumming, “Morphology of the bronchial tree in man,” *J. Appl. Physiol.*, vol. 24, no. 3, pp. 373–83, 1968.
- [12] R. F. Phalen, M. J. Oldham, C. B. Beaucage, T. T. Crocker, and J. D. Mortensen, “Postnatal enlargement of human tracheobronchial airways and implications for particle deposition,” *Anatom. Rec.*, vol. 212, no. 4, pp. 368–380, 1985.
- [13] C.-M. Ionescu, W. Kosiński, and R. De Keyser, “Viscoelasticity and fractal structure in a model of human lungs,” *Arch. Mech.*, vol. 62, no. 1, pp. 21–48, 2010.
- [14] D. E. Olson, G. A. Dart, and G. F. Filley, “Pressure drop and fluid flow regime of air inspired into the human lung,” *J. Appl. Physiol.*, vol. 28, no. 4, pp. 482–494, 1970.
- [15] R. Sturm, “Theoretical models of carcinogenic particle deposition and clearance in children’s lungs,” *J. Thorac. Dis.*, vol. 4, no. 4, pp. 368–376, 2012.
- [16] J. D. C. F. J. Miller, R. R. Mercer, “Lower respiratory tract structure of laboratory animals and humans: dosimetry implications,” *Aerosol. Sci. Technol.*, vol. 18, pp. 257–271, 1993.
- [17] M. G. Ménache, W. Hofmann, B. Ashgarian, and F. J. Miller, “Airway geometry models of children’s lungs for use in dosimetry modeling,” *Inhal. Toxicol.*, vol. 20, no. 2, pp. 101–126, 2008.
- [18] R. K. Calay, J. Kurujareon, and A. E. Holdø, “Numerical simulation of respiratory flow patterns within human lung,” *Respir. Physiol. Neurobiol.*, vol. 130, no. 2, pp. 201–221, 2002.
- [19] B. M. Smith, H. Traboulsi, J. H. M. Austin, A. Manichaikul, E. A. Hoffman, E. R. Bleecker, W. V. Cardoso, C. Cooper, D. J. Couper, S. M. Dashnaw, J. Guo, M. K. Han, N. N. Hansel, E. W. Hughes, D. R. J. Jr, R. E. Kanner, J. D. Kaufman, E. Klerup, C. L. Lin, K. Liu, C. M. Lo Cascio, F. J. Martinez, J. N. Nguyen, M. R. Prince, S. Rennard, S. S. Rich, L. Simon, Y. Sun, W. K. E., P. G. Woodruff, C. J. Baglole, and R. G. Barr, “Human airway branch variation and chronic obstructive pulmonary disease,” *Proc. Natl. Acad. Sci. U. S. A.*, vol. 115, no. 5, pp. E974–E981, 2018.
- [20] S. Montesantos, I. Katz, M. Pichelin, and G. Caillibotte, “The creation and statistical evaluation of a deterministic model of the human bronchial tree from HRCT images,” *PLoS One*, vol. 11, no. 12, p. e0168026, 2016.
- [21] E. R. Weibel, *Morphology of the human lung*. New York: Academic Press, 1963.

- [22] J. W. Lee, M. Y. Kang, H. J. Yang, and E. Lee, “Fluid-dynamic optimality in the generation-averaged length-to-diameter ratio of the human bronchial tree,” *Med. Biol. Engrg. Comput.*, vol. 45, no. 11, pp. 1071–1078, 2007.
- [23] C. G. Phillips and S. R. Kaye, “On the asymmetry of bifurcations in the bronchial tree,” *Respir. Physiol.*, vol. 107, no. 1, pp. 85–98, 1997.
- [24] O. G. Raabe, *Tracheobronchial geometry: human, dog, rat, hamster—a compilation of selected data from the project respiratory tract deposition models*. US Energy Research and Development Administration, Division of Biomedical and Environmental Research, 1976.
- [25] R. F. Phalen, H. C. Yeh, G. M. Schum, and O. G. Raabe, “Application of an idealized model to morphometry of the mammalian tracheobronchial tree,” *Anatom. Rec.*, vol. 190, no. 2, pp. 167–176, 1978.
- [26] E. R. Weibel, A. F. Cournand, and D. W. Richards, *Morphometry of the human lung*. Springer, 2014.
- [27] B. J. West, V. Bhargava, and A. L. Goldberger, “Beyond the principle of similitude: renormalization in the bronchial tree,” *J. Appl. Physiol.*, vol. 60, no. 3, pp. 1089–1097, 1986.
- [28] D. W. Thompson, *Growth and Form*. New York: Macmillan, 1942. pp. 948–957.
- [29] B. Mauroy and P. Bokov, “The influence of variability on the optimal shape of an airway tree branching asymmetrically,” *Phys. Biol.*, vol. 7, no. 1, p. 016007, 2010.
- [30] S. Gheorghiu, S. Kjelstrup, P. Pfeifer, and M.-O. Coppens, “Is the lung an optimal gas exchanger?,” in *Fractals in biology and medicine*, pp. 31–42, Springer, 2005.
- [31] P. Harper, S. S. Kraman, H. Pasterkamp, and G. R. Wodicka, “An acoustic model of the respiratory tract,” *IEEE transactions on biomedical engineering*, vol. 48, no. 5, pp. 543–550, 2001.
- [32] B. Mauroy, “3d hydrodynamics in the upper human bronchial tree: Interplay between geometry and flow distribution,” in *Fractals in biology and medicine*, pp. 43–53, Springer, 2005.
- [33] E. R. Weibel, “Mandelbrot’s fractals and the geometry of life: A tribute to benoît mandelbrot on his 80 th birthday,” in *Fractals in Biology and Medicine*, pp. 3–16, Springer, 2005.

- [34] K. Horsfield, G. Dart, D. E. Olson, G. F. Filley, and G. Cumming, “Models of the human bronchial tree,” *J. Appl. Physiol.*, vol. 31, no. 2, pp. 207–217, 1971.
- [35] J. Mead, “Contribution of compliance of airways to frequency-dependent behavior of lungs,” *J. Appl. Physiol.*, vol. 26, no. 5, pp. 670–673, 1969.
- [36] B. Ferris Jr, J. Mead, and L. Opie, “Partitioning of respiratory flow resistance in man,” *Journal of Applied Physiology*, vol. 19, no. 4, pp. 653–658, 1964.
- [37] M. Ochs, J. R. Nyengaard, A. Jung, L. Knudsen, M. Voigt, T. Wahlers, J. Richter, and H. J. G. Gundersen, “The number of alveoli in the human lung,” *Am. J. Respir. Crit. Care Med.*, vol. 169, no. 1, pp. 120–124, 2004.
- [38] A. Hislop, J. Wigglesworth, and R. Desai, “Alveolar development in the human fetus and infant,” *Early human development*, vol. 13, no. 1, pp. 1–11, 1986.
- [39] E. R. Weibel and B. W. Knight, “A morphometric study on the thickness of the pulmonary air-blood barrier,” *J. Cell Biol.*, vol. 21, no. 3, pp. 367–384, 1964.
- [40] J. E. Hall, *Guyton and Hall Textbook of Medical Physiology: Enhanced E-book*. Elsevier Health Sciences, 2010.
- [41] C. H. Liu, S. C. Niranjana, J. W. Clark, K. Y. San, J. B. Zwischenberger, A. Bidani, *et al.*, “Airway mechanics, gas exchange, and blood flow in a nonlinear model of the normal human lung,” *J. Appl. Physiol.*, vol. 84, no. 4, pp. 1447–1469, 1998.
- [42] G. L. Warren, K. J. Cureton, W. F. Middelndorf, C. A. Ray, and J. A. Warren, “Red blood cell pulmonary capillary transit time during exercise in athletes,” *Med. Sci. Sports Exerc.*, vol. 23, no. 12, p. 1353, 1991.
- [43] A. Hill, “The heat produced in contracture and muscular tone,” *The Journal of physiology*, vol. 40, no. 5, pp. 389–403, 1910.
- [44] M. Sharan, M. P. Singh, and A. Aminataei, “A mathematical model for the computation of the oxygen dissociation curve in human blood,” *BioSystems*, vol. 22, pp. 249–260, 1989.
- [45] F. Meade, “A formula for the carbon dioxide dissociation curve,” *Br. J. Anaesth.*, vol. 44, p. 630, 1972.
- [46] J. H. Comroe, R. E. Forster, A. B. Dubois, W. A. Briscoe, and E. Carlsen, *The Lung*. Chicago: Year Book, 2nd ed., 1963.

- [47] R. A. Rhoades and D. R. Bell, *Medical physiology: Principles for clinical medicine*. Lippincott Williams & Wilkins, 2013.
- [48] Medscape, “Lung anatomy,” 2017.
- [49] K. Flegal and T. Cole, “Construction of lms parameters for the centers for disease control and prevention 2000 growth chart,” August 2009.
- [50] H.-C. Yeh and G. Schum, “Models of human lung airways and their application to inhaled particle deposition,” *Bulletin of mathematical biology*, vol. 42, no. 3, pp. 461–480, 1980.
- [51] E. R. Weibel, C. C. W. Hsia, and M. Ochs, “How much is there really? why stereology is essential in lung morphometry,” *Journal of Applied Physiology*, vol. 102, no. 1, pp. 459–467, 2007.
- [52] E. R. Weibel and D. M. Gomez, “A principle for counting tissue structures on random sections,” *Journal of Applied Physiology*, vol. 17, no. 2, pp. 343–348, 1962.
- [53] D. Sterio, “The unbiased estimation of number and sizes of arbitrary particles using the disector,” *Journal of microscopy*, vol. 134, no. 2, pp. 127–136, 1984.
- [54] M. Ochs, “A brief update on lung stereology,” *Journal of microscopy*, vol. 222, no. 3, pp. 188–200, 2006.
- [55] M. J. Herring, L. F. Putney, G. Wyatt, W. E. Finkbeiner, and D. M. Hyde, “Growth of alveoli during postnatal development in humans based on stereological estimation,” *Am. J. Physiol. Heart Circ. Physiol.*, 2014.
- [56] G. Davies and L. Reid, “Growth of the alveoli and pulmonary arteries in childhood,” *Thorax*, vol. 25, no. 6, pp. 669–681, 1970.
- [57] G. E. Angus and W. Thurlbeck, “Number of alveoli in the human lung,” *Journal of applied physiology*, vol. 32, no. 4, pp. 483–485, 1972.
- [58] W. M. Thurlbeck and G. E. Angus, “Growth and aging of the normal human lung,” *CHEST Journal*, vol. 67, no. 2_Supplement, pp. 3S–7S, 1975.
- [59] P. Quanjer, G. Tammeling, J. Cotes, O. Pedersen, R. Peslin, and J.-C. Yernault, “Lung volumes and forced ventilatory flows,” *Eur Respir J*, vol. 6, pp. 5–40, 1993.
- [60] J. Stocks and P. Quanjer, “Reference values for residual volume, functional residual capacity and total lung capacity,” *Eur Respir J*, vol. 8, pp. 492–506, 1995.

- [61] P. Auld, N. Nelson, R. Cherry, A. Rudolph, and C. Smith, "Measurement of thoracic gas volume in the newborn infant," *Journal of Clinical Investigation*, vol. 42, no. 4, 1963.
- [62] W. Hofmann, "Mathematical model for the postnatal growth of the human lung," *Respiration physiology*, vol. 49, no. 1, pp. 115–129, 1982.
- [63] I. e. a. Beardsell, *MCEM Part A:MCQs*. London: Royal Society of Medicine Press, 2009.
- [64] W. F. Ganong, *Review of medical physiology*. Boston: McGraw-Hill, 2003.
- [65] E. Britannica, "Tidal volume," 2019.
- [66] I. Engström, P. Karlberg, and S. KRAEPELLEN, "Respiratory studies in children i. lung volumes in healthy children, 6–14 years of age 1," *Acta paediatrica*, vol. 45, no. 3, pp. 277–294, 1956.
- [67] C. D. Cook and J. F. Hamann, "Relation of lung volumes to height in healthy persons between the ages of 5 and 38 years," *The Journal of pediatrics*, vol. 59, no. 5, pp. 710–714, 1961.
- [68] K. Engstrom, S. C. Karlberg, and C. Swartz, "Relationship between mechanical properties of the lungs, lung volumes and ventilatory capacity in healthy children 7–15 years of age," *Acta Paediatr*, vol. 51, pp. 68–68, 1962.
- [69] C. F. Doershuk, T. D. Downs, L. W. Matthews, and M. D. Lough, "A method for ventilatory measurements in subjects 1 month–5 years of age: normal results and observations in disease," *Pediatric research*, vol. 4, no. 2, p. 165, 1970.
- [70] D. Hatch and B. Taylor, "Thoracic gas volume in early childhood.," *Archives of disease in childhood*, vol. 51, no. 11, pp. 859–864, 1976.
- [71] J. Stocks and S. Godfrey, "Specific airway conductance in relation to post-conceptual age during infancy," *Journal of Applied Physiology*, vol. 43, no. 1, pp. 144–154, 1977.
- [72] A. Greenough, J. Stocks, U. Nothen, and R. Helms, "Total respiratory compliance and functional residual capacity in young children," *Pediatric pulmonology*, vol. 2, no. 6, pp. 321–326, 1986.
- [73] C. M. Roberts, K. D. MacRae, A. J. Winning, L. Adams, and W. A. Seed, "Reference values and prediction equations for normal lung function in a non-smoking white urban population.," *Thorax*, vol. 46, no. 9, pp. 643–650, 1991.

- [74] R. S. Tepper, T. Reister, C. Angelicchio-Keller, and J. Kisling, “Forced expiratory flows and lung volumes in normal infants,” *Pediatric pulmonology*, vol. 15, no. 6, pp. 357–361, 1993.
- [75] I. Merth, J. De Winter, G. Borsboom, and P. H. Quanjer, “Pulmonary function during the first year of life in healthy infants born prematurely,” *European Respiratory Journal*, vol. 8, no. 7, pp. 1141–1147, 1995.
- [76] K. S. McCoy, R. G. Castile, E. D. Allen, D. A. Filbrun, R. L. Flucke, and E. Bar-Yishay, “Functional residual capacity (frc) measurements by plethysmography and helium dilution in normal infants,” *Pediatric pulmonology*, vol. 19, no. 5, pp. 282–290, 1995.
- [77] E. Williams, R. Hamilton, L. Sutton, J. Viale, and C. Hahn, “Alveolar and dead space volume measured by oscillations of inspired oxygen in awake adults,” *American journal of respiratory and critical care medicine*, vol. 156, no. 6, pp. 1834–1839, 1997.
- [78] J. Roca, F. Burgos, J. Barbera, J. Sunyer, R. Rodriguez-Roisin, J. Castell-sague, J. Sanchis, J. Antoo, P. Casan, and J. Clausen, “Prediction equations for plethysmographic lung volumes,” *Respiratory medicine*, vol. 92, no. 3, pp. 454–460, 1998.
- [79] J. A. Neder, S. Andreoni, A. Castelo-Filho, and L. E. Nery, “Reference values for lung function tests: I. static volumes,” *Brazilian Journal of Medical and Biological Research*, vol. 32, no. 6, pp. 703–717, 1999.
- [80] P. J. Cordero, P. Morales, E. Benlloch, L. Miravet, and J. Cebrian, “Static lung volumes: reference values from a latin population of spanish descent,” *Respiration*, vol. 66, no. 3, pp. 242–250, 1999.
- [81] R. Castile, D. Filbrun, R. Flucke, W. Franklin, and K. McCoy, “Adult-type pulmonary function tests in infants without respiratory disease,” *Pediatric pulmonology*, vol. 30, no. 3, pp. 215–227, 2000.
- [82] A. Schibler, G. Hall, F. Businger, B. Reinmann, J. Wildhaber, M. Cernelc, and U. Frey, “Measurement of lung volume and ventilation distribution with an ultrasonic flow meter in healthy infants,” *European Respiratory Journal*, vol. 20, no. 4, pp. 912–918, 2002.
- [83] G. Hulskamp, A.-f. Hoo, H. Ljungberg, S. Lum, J. J. Pillow, and J. Stocks, “Progressive decline in plethysmographic lung volumes in infants: physiology or technology?,” *American journal of respiratory and critical care medicine*, vol. 168, no. 8, pp. 1003–1009, 2003.

- [84] G. Polgar and P. Varuni, *Pulmonary function testing in children: techniques and standards*. Saunders Limited., 1971.
- [85] L. D. Wood, S. Prichard, T. Weng, K. Kruger, A. Bryan, and H. Levison, "Relationship between anatomic dead space and body size in health, asthma, and cystic fibrosis 1–3," *American Review of Respiratory Disease*, vol. 104, no. 2, pp. 215–222, 1971.
- [86] J. Nunn, E. Campbell, and B. Peckett, "Anatomical subdivisions of the volume of respiratory dead space and effect of position of the jaw," *Journal of Applied Physiology*, vol. 14, no. 2, pp. 174–176, 1959.
- [87] E. P. Radford, "Ventilation standards for use in artificial respiration," *Journal of applied physiology*, vol. 7, no. 4, pp. 451–460, 1955.
- [88] W. S. Fowler, "Lung function studies. II. The respiratory dead space," *Am. J. Physiol.*, vol. 154, no. 3, pp. 405–416, 1948.
- [89] G. Birath, "Respiratory dead space measurements in a model lung and healthy human subjects according to the single breath method," *J. Appl. Physiol.*, vol. 14, pp. 517–520, July 1959.
- [90] E. Harris, M. E. Hunter, E. R. Seelye, M. Vedder, and R. Whitlock, "Prediction of the physiological dead-space in resting normal subjects," *Clinical Science*, vol. 45, no. 3, pp. 375–386, 1973.
- [91] S. Lewis and C. J. Martin, "Characteristics of the washout dead space," *Resp. Physiol.*, vol. 36, no. 1, pp. 51–63, 1979.
- [92] E. M. Williams, R. M. Hamilton, L. Sutton, J. P. Viale, and C. E. W. Hahn, "Alveolar and dead space volume measured by oscillations of inspired oxygen in awake adults," *Am. J. Respir. Crit. Care Med.*, vol. 156, no. 6, pp. 1834–1839, 1997.
- [93] Y. Tang, M. J. Turner, and A. B. Baker, "A new equal area method to calculate and represent physiologic, anatomical, and alveolar dead spaces," *Anesthesiology*, vol. 104, no. 4, pp. 696–700, 2006.
- [94] R. A. Epstein and A. I. Hyman, "Ventilatory requirements of critically ill neonates," *Anesthesiology*, vol. 53, no. 5, pp. 379–384, 1980.
- [95] T. Gerhardt and E. Bancalari, "Apnea of prematurity: I. Lung function and regulation of breathing," *Pediatrics*, vol. 74, no. 1, pp. 58–62, 1984.
- [96] K. Sandberg, B. A. Sjöqvist, O. Hjalmarson, and T. Olsson, "Efficiency of ventilation in neonatal pulmonary maladaptation," *Acta Paediatr.*, vol. 76, no. 1, pp. 30–36, 1987.

- [97] D. Lagneaux, C. Mossay, F. Geubelle, and G. Christiaens, “Alveolar data in healthy, awake neonates during spontaneous ventilation: a preliminary investigation,” *Pediatr. Pulmonol.*, vol. 5, no. 4, pp. 225–231, 1988.
- [98] U. Wenzel, R. R. Wauer, and G. Schmalisch, “Comparison of different methods for dead space measurements in ventilated newborns using CO₂-volume plot,” *Intensive Care Med.*, vol. 25, no. 7, pp. 705–713, 1999.
- [99] T. Dassios, P. Dixon, A. Hickey, S. Fouzas, and A. Greenough, “Physiological and anatomical dead space in mechanically ventilated newborn infants,” *Pediatr. Pulmonol.*, vol. 53, no. 1, pp. 57–63, 2018.
- [100] A. B. Dubois, S. Y. Botelho, and J. Comroe, J. H., “A new method for measuring airway resistance in man using a body plethysmograph: values in normal subjects and in patients with respiratory disease,” *J. Clin. Invest.*, vol. 35, no. 3, pp. 327–335, 1956.
- [101] H. Bachofen, “Lung tissue resistance and pulmonary hysteresis,” *J. Appl. Physiol.*, vol. 24, no. 3, pp. 296–301, 1968.
- [102] A. A. Viljanen, B. C. Viljanen, P. K. Halttunen, and K.-E. Kreuz, “Body plethysmographic studies in non-smoking, healthy adults,” *Scand. J. Clin. Lab. Invest.*, vol. 42, no. sup159, pp. 35–50, 1982.
- [103] Z. Hantos, B. Daroczy, B. Suki, G. Galgoczy, and T. Csendes, “Forced oscillatory impedance of the respiratory system at low frequencies,” *J. Appl. Physiol.*, vol. 60, no. 1, pp. 123–132, 1986.
- [104] D. W. Kaczka, E. P. Ingenito, B. Suki, and K. R. Lutchen, “Partitioning airway and lung tissue resistances in humans: effects of bronchoconstriction,” *J. Appl. Physiol.*, vol. 82, no. 5, pp. 1531–1541, 1997.
- [105] B. Koch, N. Friedrich, H. Völzke, R. A. Jörres, S. B. Felix, R. Ewert, C. Schaeper, and S. Gläser, “Static lung volumes and airway resistance reference values in healthy adults,” *Respirology*, vol. 18, no. 1, pp. 170–178, 2013.
- [106] S. Verbanck, A. Van Muylem, D. Schuermans, I. Bautmans, B. Thompson, and W. Vincken, “Transfer factor, lung volumes, resistance and ventilation distribution in healthy adults,” *Eur. Respir. J.*, vol. 47, pp. 166–176, 2016.
- [107] C. D. Cook, J. M. Sutherland, S. Segal, R. B. Cherry, J. Mead, M. B. McIlroy, and C. A. Smith, “Studies of respiratory physiology in the newborn infant. III. Measurements of mechanics of respiration,” *J. Clin. Investig.*, vol. 36, no. 3, pp. 440–448, 1957.

- [108] P. R. Swyer, R. C. Reiman, and J. J. Wright, "Ventilation and ventilatory mechanics in the newborn: methods and results in 15 resting infants," *J. Pediatr.*, vol. 56, no. 5, pp. 612–622, 1960.
- [109] G. Polgar, "Airway resistance in the newborn infant: preliminary communication," *J. Pediatr.*, vol. 59, no. 6, pp. 915–921, 1961.
- [110] P. Karlberg and G. Koch, "Respiratory studies in newborn infants. III.: Development of mechanics of breathing during the first week of life. A longitudinal study 1," *Acta Paediatr.*, vol. 51, pp. 121–129, 1962.
- [111] G. Polgar and G. P. Kong, "The nasal resistance of newborn infants," *J. Pediatr.*, vol. 67, no. 4, pp. 557–567, 1965.
- [112] E. D. Burnard, P. Grattan-Smith, C. G. Picton-Warlow, and A. Grauaug, "Pulmonary insufficiency in prematurity," *J. Paediatr. Child Health*, vol. 1, no. 1, pp. 12–38, 1965.
- [113] G. Polgar and S. T. String, "The viscous resistance of the lung tissues in newborn infants," *J. Pediatr.*, vol. 69, no. 5, pp. 787–792, 1966.
- [114] M. E. B. Wohl, L. C. Stigol, and J. Mead, "Resistance of the total respiratory system in healthy infants and infants with bronchiolitis," *Pediatrics*, vol. 43, no. 4, pp. 495–509, 1969.
- [115] M. Radford, "Measurement of airway resistance and thoracic gas volume in infancy," *Arch. Dis. Child.*, vol. 49, no. 8, pp. 611–615, 1974.
- [116] J. Stocks, N. M. Levy, and S. Godfrey, "A new apparatus for the accurate measurement of airway resistance in infancy," *J. Appl. Physiol.*, vol. 43, no. 1, pp. 155–159, 1977.
- [117] M. R. Thomas, G. F. Rafferty, R. Blowes, J. L. Peacock, N. Marlow, S. Calvert, A. Milner, and A. Greenough, "Plethysmograph and interrupter resistance measurements in prematurely born young children," *Arch. Dis. Child Fetal Neonatal Ed.*, vol. 91, no. 3, pp. F193–F196, 2006.
- [118] O. Battisti, J. M. Bertrand, H. Rouatbi, and G. Escandar, "Lung compliance and airways resistance in healthy neonates," *Pediatr. Therapeut.*, vol. 2, p. 1000114, 2012.